



HAL
open science

Environmental drivers of under-ice phytoplankton bloom dynamics in the Arctic Ocean

Mathieu Ardyna, C.J. Mundy, Matthew M. Mills, Laurent Oziel, Pierre-Luc Grondin, Leo Lacour, Gauthier Verin, Gert van Dijken, Josephine Ras, Eva Alou-Font, et al.

► **To cite this version:**

Mathieu Ardyna, C.J. Mundy, Matthew M. Mills, Laurent Oziel, Pierre-Luc Grondin, et al.. Environmental drivers of under-ice phytoplankton bloom dynamics in the Arctic Ocean. *Elementa: Science of the Anthropocene*, 2020, 8 (1), pp.30. 10.1525/elementa.430 . hal-03095648

HAL Id: hal-03095648

<https://hal.science/hal-03095648>

Submitted on 4 Jan 2021

HAL is a multi-disciplinary open access archive for the deposit and dissemination of scientific research documents, whether they are published or not. The documents may come from teaching and research institutions in France or abroad, or from public or private research centers.

L'archive ouverte pluridisciplinaire **HAL**, est destinée au dépôt et à la diffusion de documents scientifiques de niveau recherche, publiés ou non, émanant des établissements d'enseignement et de recherche français ou étrangers, des laboratoires publics ou privés.

RESEARCH ARTICLE

Environmental drivers of under-ice phytoplankton bloom dynamics in the Arctic Ocean

Mathieu Ardyna^{*†}, C. J. Mundy[‡], Matthew M. Mills^{*}, Laurent Oziel^{†,§,||}, Pierre-Luc Grondin^{§,||}, Léo Lacour^{§,||}, Gauthier Verin^{§,||}, Gert van Dijken^{*}, Joséphine Ras[†], Eva Alou-Font[¶], Marcel Babin^{§,||}, Michel Gosselin^{**}, Jean-Éric Tremblay^{§,||}, Patrick Raimbault^{††}, Philipp Assmy^{‡‡}, Marcel Nicolaus^{§§}, Hervé Claustre[†] and Kevin R. Arrigo^{*}

The decline of sea-ice thickness, area, and volume due to the transition from multi-year to first-year sea ice has improved the under-ice light environment for pelagic Arctic ecosystems. One unexpected and direct consequence of this transition, the proliferation of under-ice phytoplankton blooms (UIBs), challenges the paradigm that waters beneath the ice pack harbor little planktonic life. Little is known about the diversity and spatial distribution of UIBs in the Arctic Ocean, or the environmental drivers behind their timing, magnitude, and taxonomic composition. Here, we compiled a unique and comprehensive dataset from seven major research projects in the Arctic Ocean (11 expeditions, covering the spring sea-ice-covered period to summer ice-free conditions) to identify the environmental drivers responsible for initiating and shaping the magnitude and assemblage structure of UIBs. The temporal dynamics behind UIB formation are related to the ways that snow and sea-ice conditions impact the under-ice light field. In particular, the onset of snowmelt significantly increased under-ice light availability ($>0.1\text{--}0.2$ mol photons $\text{m}^{-2} \text{d}^{-1}$), marking the concomitant termination of the sea-ice algal bloom and initiation of UIBs. At the pan-Arctic scale, bloom magnitude (expressed as maximum chlorophyll *a* concentration) was predicted best by winter water $\text{Si}(\text{OH})_4$ and PO_4^{3-} concentrations, as well as $\text{Si}(\text{OH})_4:\text{NO}_3^-$ and $\text{PO}_4^{3-}:\text{NO}_3^-$ drawdown ratios, but not NO_3^- concentration. Two main phytoplankton assemblages dominated UIBs (diatoms or *Phaeocystis*), driven primarily by the winter nitrate:silicate ($\text{NO}_3^-:\text{Si}(\text{OH})_4$) ratio and the under-ice light climate. *Phaeocystis* co-dominated in low $\text{Si}(\text{OH})_4$ (i.e., $\text{NO}_3^-:\text{Si}(\text{OH})_4$ molar ratios >1) waters, while diatoms contributed the bulk of UIB biomass when $\text{Si}(\text{OH})_4$ was high (i.e., $\text{NO}_3^-:\text{Si}(\text{OH})_4$ molar ratios <1). The implications of such differences in UIB composition could have important ramifications for Arctic biogeochemical cycles, and ultimately impact carbon flow to higher trophic levels and the deep ocean.

Keywords: Under-ice phytoplankton blooms; Biogeochemical cycles; Nutrients; Sea Ice; Climate change; Arctic Ocean

1. Introduction

The Arctic Ocean (AO) is changing profoundly, with drastic reductions in both sea-ice area and thickness (Kwok, 2018; Stroeve and Notz, 2018). Since 1979, the summer sea-ice extent has declined by $>40\%$, with first-year ice replacing the once prevalent multiyear ice pack (AMAP,

2017). Sea-ice melt is beginning earlier in the year while freeze-up is delayed; consequently, more solar radiation is reaching the upper ocean now than it has in the past (Nicolaus et al., 2012; Arndt and Nicolaus, 2014; Katlein et al., 2019). Such modifications result in a substantially thinner sea-ice cover that is more prone to deformation

* Department of Earth System Science, Stanford University, Stanford, CA, US

† Sorbonne Université, CNRS, Laboratoire d'Océanographie de Villefranche, LOV, Villefranche-sur-Mer, FR

‡ Centre for Earth Observation Science (CEOS), University of Manitoba, Winnipeg, Manitoba, CA

§ Takuvik Joint International Laboratory, Laval University (Canada) – CNRS, FR

|| Département de biologie et Québec-Océan, Université Laval, Québec, Québec, CA

[¶] Balearic Islands Coastal Observing and Forecasting System (SOCIB), Palma de Mallorca, ES

** Institut des sciences de la mer de Rimouski, Université du Québec à Rimouski, Rimouski, Québec, CA

†† Aix-Marseille University, Mediterranean Institute of Oceanography (MIO), CNRS/INSU, IRD, Marseille, FR

‡‡ Norwegian Polar Institute, Fram Centre, Tromsø, NO

§§ Alfred Wegener Institute for Polar and Marine Research, Bremerhaven, DE

Corresponding author: Mathieu Ardyna (ardyna@stanford.edu)

and melting, favoring the formation of leads and melt ponds, respectively, and ultimately leading to increases in light transmission to the under-ice environment.

Because snow and sea ice strongly attenuate solar radiation, the growth of phytoplankton at high latitudes has long been thought to begin in the open water along sea-ice edges during the spring, when solar elevation increases and sea-ice melt stabilizes the upper water column (Wassmann et al., 1991; Sakshaug, 2004). However, changing sea-ice dynamics (e.g., extent, age and thickness) are challenging our current understanding of Arctic phytoplankton phenology (Kahru et al., 2010; Ardyna et al., 2014; Renaut et al., 2018), including the recent recognition of large under-ice blooms (UIBs). Here we define a UIB as a phytoplankton bloom that starts and develops beneath a significant concentration of sea ice (generally >50%). These blooms are distinct from sea-ice algae that become detached from the bottom sea ice (Mundy et al., 2014) and from blooms at the sea-ice edge that are advected under the sea ice (Johnsen et al., 2018). UIBs have been documented across the Arctic and are now accepted as prevalent phenological phytoplankton features over much of the Arctic Ocean (e.g., Yager et al., 2001; Fortier et al., 2002; Arrigo et al., 2012, 2014; Mundy et al., 2014; Assmy et al., 2017; Hill et al., 2018; Oziel et al., 2019). However, the main ecological drivers behind the initiation, structure and productivity of UIBs and their spatial distribution and interannual variability remain to be assessed at a pan-Arctic scale.

A complex mosaic of multiple bottom-up (i.e., light, nutrients, stratification and water temperature) and

top-down drivers (i.e., zooplankton grazing) in the Arctic is suspected to shape the unique ecological niches of UIBs. The amount of light transmitted through the sea ice, which depends on snow and sea-ice thickness, and on the presence of melt-ponds and leads, appears to be critical for UIB initiation (Arrigo et al., 2012, 2014; Assmy et al., 2017; Oziel et al., 2019). Large differences in UIB phytoplankton assemblages have also been reported in the AO, from massive diatom UIBs along the Chukchi shelf break (Arrigo et al., 2012, 2014; Laney and Sosik, 2014) to *Phaeocystis pouchetii* UIBs north of Svalbard (Assmy et al., 2017). Such differences in UIB phytoplankton assemblages are not yet fully understood and might have important repercussions on productivity, carbon export, and food web dynamics.

Within this context, and given the ongoing changes in the Arctic icescape, an integrative ecological understanding of UIBs is needed. Here, we investigated the environmental and ecological processes responsible for driving UIB initiation, magnitude, and assemblages in the AO. To achieve an integrated understanding of UIBs, observations from a total of 11 expeditions by seven major international Arctic projects were synthesized for the first time, spanning spring sea-ice-covered and summer sea-ice-free conditions (**Figure 1** and **Table 1**). Based on this large dataset, the goals of this study were to 1) delineate the environmental drivers (in both space and time) governing the occurrence of UIBs, 2) examine the assemblage diversity of UIBs and 3) consider the potential roles of UIBs in Arctic biogeochemical cycles and impacts on both pelagic and benthic Arctic ecosystems.

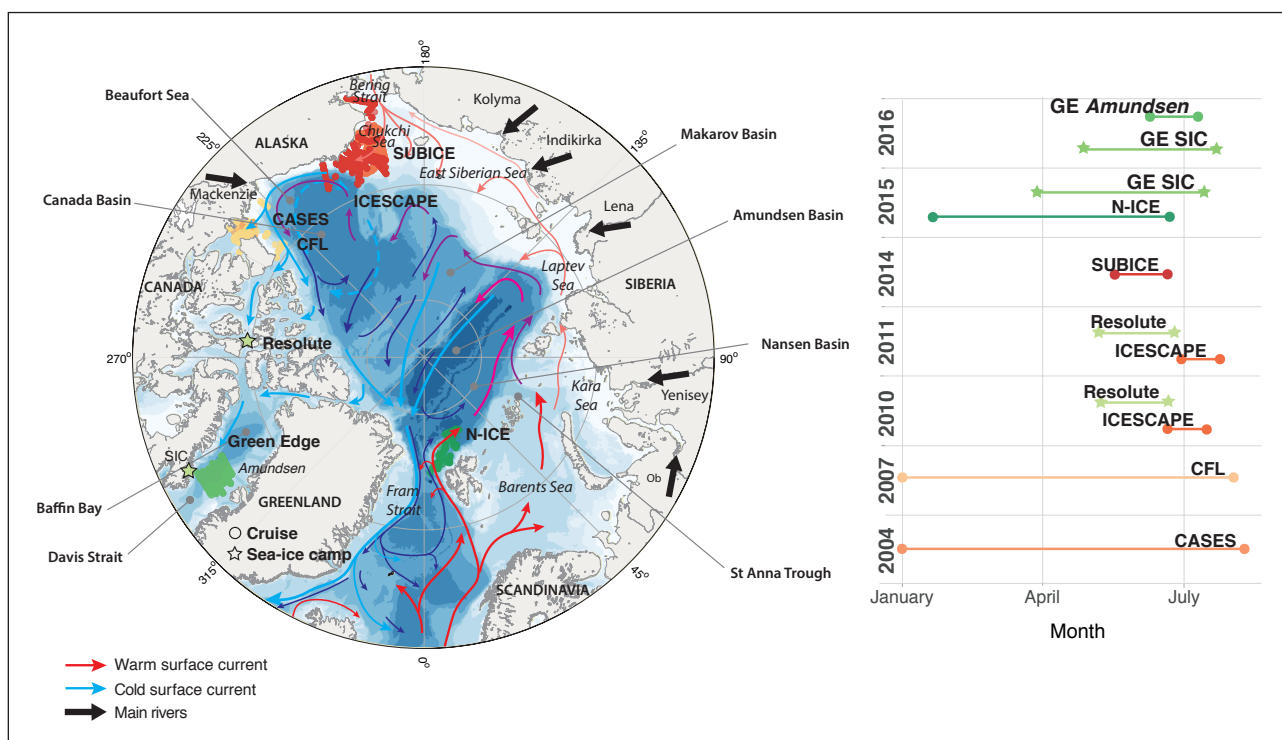


Figure 1: Location and sampling periods of the cruises (circles) and sea-ice camps (stars). Shown are the dominant Arctic Ocean currents with inflowing relatively warm surface currents (red arrows) and colder surface currents (light blue arrows), together with intermediate and deep currents (burgundy and dark blue arrows, respectively; modified from Anderson and Macdonald, 2015). Black arrows indicate the main river inputs. DOI: <https://doi.org/10.1525/elementa.430.f1>

Table 1: Projects and their expeditions (cruises and sea-ice camps) used in the present study. DOI: <https://doi.org/10.1525/elementa.430.t1>

Project	Expedition	Arctic region ^a	References
CASES	<i>Amundsen 2004</i>	Beaufort Sea	Brugel et al. (2009); Tremblay et al. (2008)
CFL	<i>Amundsen 2008</i>	Beaufort Sea	Blais et al. (2017); Mundy et al. (2009)
Green Edge	<i>Sea-Ice Camp 2015</i> <i>Sea-Ice Camp 2016</i> <i>Amundsen 2016</i>	Baffin Bay	Oziel et al. (2019); Randelhoff et al. (2019); Massicotte et al. (2020)
ICESCAPE	<i>Healy 2010</i> <i>Healy 2011</i>	Chukchi Sea	Arrigo et al. (2012, 2014)
N-ICE	<i>RV Lance 2015</i>	Nansen Basin	Assmy et al. (2017)
Resolute	<i>Sea-Ice camp 2010</i> <i>Sea-Ice camp 2011</i>	Canadian Archipelago	Mundy et al. (2014)
SUBICE	<i>Healy 2014</i>	Chukchi Sea	Arrigo et al. (2017)

^a See Figure 1 for locations of the different expeditions.

2. Materials and methods

A comprehensive dataset was compiled from 11 Arctic Ocean expeditions, including cruises and sea-ice camps (**Figure 1** and **Table 1**). This large dataset consists of 756 stations sampled between 2004 and 2016. Compared to other existing biological datasets from the Arctic Ocean (Ardyna et al., 2013; Matrai et al., 2013), this new compilation is unique, as it spans the sea-ice-covered spring and sea-ice-free summer periods and includes a diverse array of optical (e.g., under sea-ice daily vertical light profiles), hydrological (i.e., physical properties), biogeochemical (nutrient inventories) and biological (phytoplankton pigment signatures, abundance, biovolume and taxonomic composition) data.

2.1. Light and sea-ice properties

Light measurements were compiled only for datasets collected during sea-ice camps (considered as pseudo-eulerian expeditions). Vertical profiles of downwelling irradiance and upwelling radiance were collected using profiling radiometers (Mundy et al., 2014; Oziel et al., 2019). Surface albedo at the Green Edge and Resolute sea-ice camps was measured with a custom-built radiometer (Solalb, developed at Institut des Géosciences de l'Environnement) and a shortwave surface albedo sensor (Kipp & ZonenTM CNR1) (Mundy et al., 2014), respectively. Satellite-derived sea-ice concentrations were retrieved from SSMIS at 25-km resolution available from the National Snow and Ice Data Center (NSIDC, <https://nsidc.org>; Cavalieri et al., 1996). Satellite-derived sea-ice ages were derived from remotely sensed sea-ice motion and sea-ice extent (NSIDC, <https://nsidc.org>; Tschudi et al., 2019).

2.2. Water properties and nutrient inventories

At each station, a conductivity-temperature-depth (CTD) profiler, together with various sensors, was deployed to measure water temperature and salinity, as well as ancillary variables such as dissolved oxygen, nitrate (NO_3^-),

photosynthetically active radiation (PAR), and phytoplankton fluorescence. Concentrations of NO_3^- plus nitrite (NO_2^-), phosphate (PO_4^{3-}) and silicate (Si(OH)_4) were also determined at multiple depths for all expeditions. Please refer to the references listed in **Table 1** for further details on the methods used (i.e., instruments, calibrations and protocols) for each expedition. It should be noted that only nutrient data were available for the CASES expedition. The winter nutrient concentrations were defined as the maximum values in the first 100 m over the duration of each expedition. The maximum nutrient (NO_3^- , Si(OH)_4 , PO_4^{3-}) drawdowns were then determined as the difference between the winter concentration and the lowest measured concentration in the upper 100 m over the duration of the expedition. Following Newton et al. (2013) and Randelhoff et al. (2019), the “Arctic N-P relationship” (ANP) was calculated to delineate the proportion of Atlantic-versus Pacific-derived waters. Essentially, ANP = 0 means the NO_3^- - PO_4^{3-} pair falls on the regression line for Atlantic Water, whereas for ANP = 1, the pair falls on the regression line for Pacific-derived water.

2.3. Phytoplankton pigment signatures

Phytoplankton chlorophyll *a* (chl *a*) and accessory pigments were measured at multiple depths for all expeditions except the sea-ice camp in Resolute (consisting of a total of 2028 samples), using high-performance liquid chromatography (HPLC). The methods used for Green Edge and SUBICE, including information about the standards, calibration, detection limits and quantification procedures, are described in detail in Coupel et al. (2015). For the ICESCAPE, CFL and Norwegian young sea ICE (N-ICE) expeditions, full details on the methods are provided in Arrigo et al. (2014), Alou-Font et al. (2016), and Kauko et al. (2019), respectively. A list of pigments identified and quantified for this study is provided in **Table 2**. Note that for the sea-ice camp in Resolute, chl *a* concentrations were measured using a Turner Designs 10-005R fluorometer, as described in Mundy et al. (2014).

Table 2: Phytoplankton pigments and their presence in the algae groups used in this study with the CHEMTAX program. DOI: <https://doi.org/10.1525/elementa.430.t2>

Pigment	Abbreviation ^a	Specificity
Chlorophylls		
Chlorophyll <i>a</i>	Chl <i>a</i>	All phytoplankton except <i>Prochlorococcus</i>
Chlorophyll <i>b</i>	Chl <i>b</i>	Chlorophytes, prasinophytes, euglenophytes
Chlorophyll <i>c</i> ₁ + <i>c</i> ₂	Chl <i>c</i> ₁ + <i>c</i> ₂	Diatoms, prymnesiophytes, dinoflagellates, cryptophytes, chrysophytes, and raphidophytes
Chlorophyll <i>c</i> ₃	Chl <i>c</i> ₃	Prymnesiophytes, chrysophytes and dinoflagellates type 2 (lacking peridinin)
Xanthophylls		
19'-butanoyloxyfucoxanthin	But-fuco	Prymnesiophytes, chrysophytes, and dinoflagellates type 2 (lacking peridinin)
Fucoxanthin	Fuco	Diatoms, prymnesiophytes, chrysophytes, pelagophytes, and dinoflagellates type 2 (lacking peridinin)
19'-hexanoyloxyfucoxanthin	Hex-fuco	Major in prymnesiophytes and dinoflagellates type 2 (lacking peridinin)
Lutein	Lut	Chlorophytes, prasinophytes
Neoxanthin	Neo	Chlorophytes, prasinophytes
Peridinin	Peri	Dinoflagellates type 1
Prasinoxanthin	Pras	Prasinophytes type 3 (A, B)

^aAbbreviations from the Scientific Council for Oceanic Research (Jeffrey et al., 1997).

CHEMTAX software (Mackey et al., 1996) was utilized to determine the relative abundance of distinct algal groups relative to total chl *a* from *in situ* pigment measurements. The CHEMTAX software is based on a factorization program that uses “best guess” ratios of accessory pigments to chl *a* for each phytoplankton taxon. These ratios are based on marker pigment concentrations of algal groups that are known to be present in the Arctic Ocean (Vidussi et al., 2004; Coupel et al., 2015). The program uses a steepest descent algorithm to obtain the best fit to the data based on assumed ratios of pigment to chl *a* (for more detail, see Mackey et al., 1996). As CHEMTAX is sensitive to the *a priori* groupings of the initial ratio matrix (Latasa, 2007), the later version (v1.95) was used to obtain more stable output matrices (Wright et al., 2009). In this CHEMTAX version, the initial matrices are optimized by generating 60 further pigment ratio tables using a random function (RAND in Microsoft Excel) as described in Wright et al. (2009). The results of the six best output matrices (with the smallest residuals, equivalent to 10% of all matrices) were used to calculate the averages of the relative abundance estimates and final pigment ratios.

The choices of the initial pigment ratio and the algal groups (Table 2) were made according to previous chemotaxonomic studies conducted in the Arctic Ocean (Vidussi et al., 2004; Coupel et al., 2015), the Labrador Sea (Fragoso et al., 2017), and the global ocean (Higgins et al., 2011). The algal groups were clustered into nine chemotaxonomic classes (see Table 3). The pigment ratios for dinoflagellates and cryptophytes were selected from Vidussi et al. (2004), diatoms and chryso-pelagophytes from Coupel et al. (2015), the haptophyte *Phaeocystis* from Antajan et al. (2004), and the others from Higgins et al. (2011).

2.4. Phytoplankton abundance, biovolume and taxonomic composition

Imaging FlowCytobots (IFCBs) were used in parallel with CHEMTAX for the identification and enumeration of nano- and microphytoplankton (see Olson and Sosik, 2007, and Laney and Sosik, 2014, for the specifications of these instruments) in several expeditions (ICESCAPE, SUBICE and Green Edge). The targeted size range was 1–150 μm , although the image resolution of ~ 3.4 pixels μm^{-1} limited the identification of < 10 μm cells to broad functional groups. The same method was used for the Green Edge, ICESCAPE and SUBICE expeditions. Briefly, image processing followed the protocol described by Sosik and Olson (2007) with a custom MATLAB (2013b) code (<https://github.com/hsosik/ifcb-analysis>). The classification step and the machine-learning algorithm of the Ecotaxa application were used (Picheral et al., 2017). After automatic identification, each object was either validated visually or corrected. Within these image libraries, only living objects were kept for further analyses (images with a bad focus, air bubbles, or detritus were removed). Finally, the biovolume of each IFCB-imaged cell was computed according to Moberg and Sosik (2012).

2.5. Statistical analysis

The Kruskal-Wallis H test was used to test for significant differences in nutrient concentrations and ratios between the different expeditions. A correlation matrix (based on Spearman's ρ) was also produced between the major algal groups and the environmental drivers and visualized as a heatmap. All statistical analyses were performed using the software package R version 3.6.

Table 3: Matrix of ratios of accessory pigment to chlorophyll *a* for different algal groups. DOI: <https://doi.org/10.1525/elementa.430.t3>

Class ^a	Chl <i>b</i>	Chl <i>c</i> ₃	Fuco	Peri	Allo	But-fuco	Hex-fuco	Chl <i>c</i> ₁₊₂	Neo	Pras	Lut
Initial ratio matrix ^b											
Diatoms	0	0	0.425	0	0	0	0	0.171	0	0	0
Dinoflagellates	0	0	0	0.6	0	0	0	0	0	0	0
Cryptophytes	0	0	0	0	0.673	0	0	0	0	0	0
Chryso-Pelago	0	0.114	0.285	0	0	0.831	0	0.285	0	0	0
Prasino-2	0.812	0	0	0	0	0	0	0	0.033	0	0.096
Prasino-3	0.764	0	0	0	0	0	0	0	0.078	0.248	0.009
Chlorophytes	0.339	0	0	0	0	0	0	0	0.036	0	0.187
<i>Phaeocystis</i>	0	0.208	0.35	0	0	0	0	0	0	0	0
Hapto-7	0	0.171	0.259	0	0	0.013	0.491	0.276	0	0	0
Final ratio matrix ^c											
Diatoms	0	0	0.455	0	0	0	0	0.173	0	0	0
Dinoflagellates	0	0	0	0.583	0	0	0	0	0	0	0
Cryptophytes	0	0	0	0	0.620	0	0	0	0	0	0
Chryso-Pelago	0	0.089	0.302	0	0	0.982	0	0.257	0	0	0
Prasino-2	0.943	0	0	0	0	0	0	0	0.038	0	0.068
Prasino-3	0.661	0	0	0	0	0	0	0	0.096	0.328	0.010
Chlorophytes	0.349	0	0	0	0	0	0	0	0.037	0	0.162
<i>Phaeocystis</i>	0	0.402	0.465	0	0	0	0	0	0	0	0
Hapto-7	0	0.134	0.226	0	0	0.013	0.760	0.237	0	0	0

^a Designations according to Higgins et al. (2011), where Chryso-Pelago indicates chrysophytes and pelagophytes; Hapto-7, haptophytes type 7; Prasino-3, prasinophytes type 3; and Prasino-2, prasinophytes type 2.

^b Initial ratio matrix retrieved for diatoms and Chryso-Pelago from Coupel et al. (2015), for dinoflagellates, cryptophytes, and Hapto-7 from Vidussi et al. (2004), for Prasino-2, Prasino-3, and chlorophytes from Higgins et al. (2011), and for *Phaeocystis* from Antajan et al. (2004).

^c Final ratio matrix obtained after CHEMTAX optimization between the *in situ* pigment concentrations and the initial ratio matrix.

3. Results

3.1. Sea-ice, light, hydrography and nutrient conditions

All of the sea ice sampled in this study was first year sea ice. However, sea-ice conditions varied with each expedition and from station to station in terms of type, thickness, and optical properties. Sea-ice concentrations derived from satellite-derived observations (Figures 2 and 3) show that for the SUBICE and N-ICE expeditions, more than 90% of the stations were sea-ice-covered (>50% sea-ice concentration; Figure 2C, D). However, only 56, 44, 37, 22, and 12% of the stations were sea-ice-covered for CASES, CFL, GE *Amundsen* and ICESCAPE 1 and 2 expeditions, respectively (Figure 2A, B and E, F). Sampling from an ice camp requires consolidated sea ice (~100% sea-ice concentration) and usually stops just before ice breakup (for obvious safety concerns). However, fixed sampling allowed for time-series of snow and sea-ice properties (albedo, thickness, etc.) in much more detail than using “destructive” icebreakers. All sea-ice camps (Resolute 2010 and Green Edge 2015, 2016) were conducted on landfast sea ice

(Figure 3). Before the melting periods, sea-ice thickness was similar for all ice camp expeditions, ranging from 1.0 to 1.4 m (Figure 4D–F). However, snow depth on top of the sea ice varied greatly. For instance, the average snow depth before melt was ~14, 40 and 30 cm (Figure 4D–F), respectively, for the three ice camps. This large variability in snow cover had little impact on surface albedo (~0.9 before melt for all ice camps; Figure 4A–C) but largely controlled under-ice light transmittance (0.13, 0.06, 0.11 mol photons m⁻² d⁻¹ at 2 m under the ice bottom, respectively for the three ice camps Figure 4G, H). Sea-ice algae also contributed to the reduction of under-ice PAR, albeit to a lesser degree than snow cover.

In terms of water masses, both Atlantic- and Pacific-derived waters were included in our dataset (Figure 5), from the western AO (i.e., Chukchi and Beaufort Seas) where water masses carried a strong Pacific signature (indicated in blue; Figure 5B) to the eastern AO (i.e., north of Svalbard) influenced by Atlantic-derived waters (shown in red; Figure 5A). In Baffin Bay, a clear gradient exists

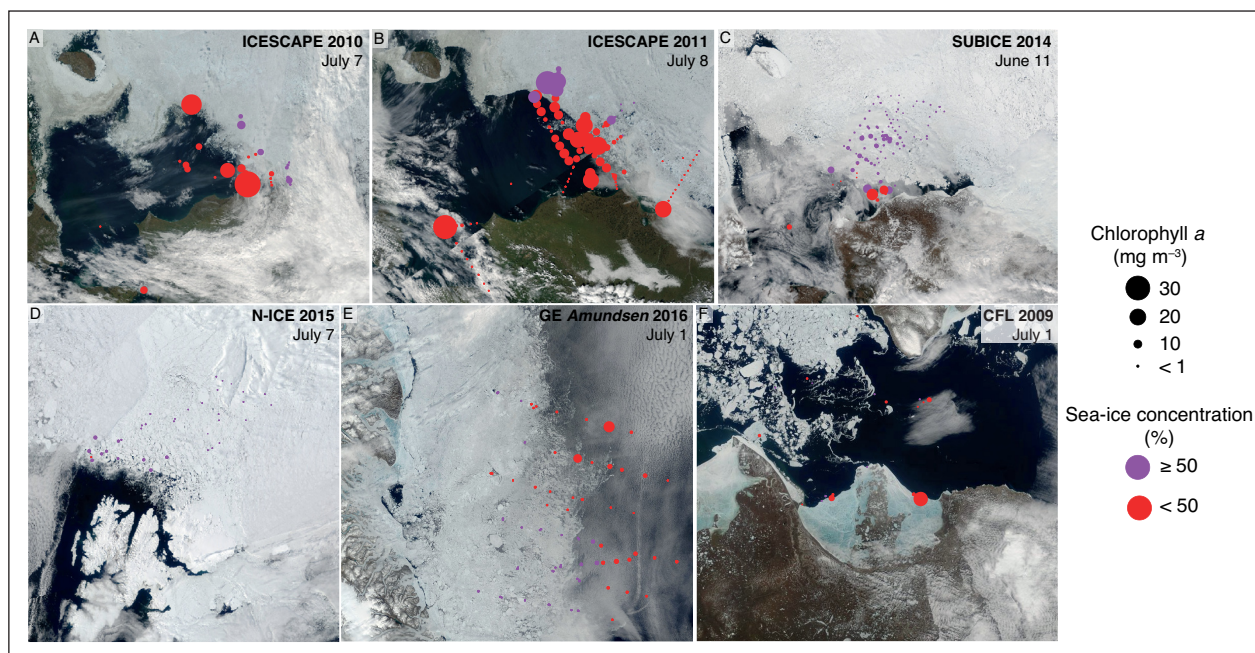


Figure 2: Terra MODIS satellite images showing locations of the different cruises. The date of the image was at the approximate peak of the phytoplankton bloom (maximum chl *a* concentration, as depicted by the size of the circles; mg m^{-3}). Red and purple indicate sea-ice concentration on the date of the sampling, $<50\%$ and $\geq 50\%$, respectively. DOI: <https://doi.org/10.1525/elementa.430.f2>

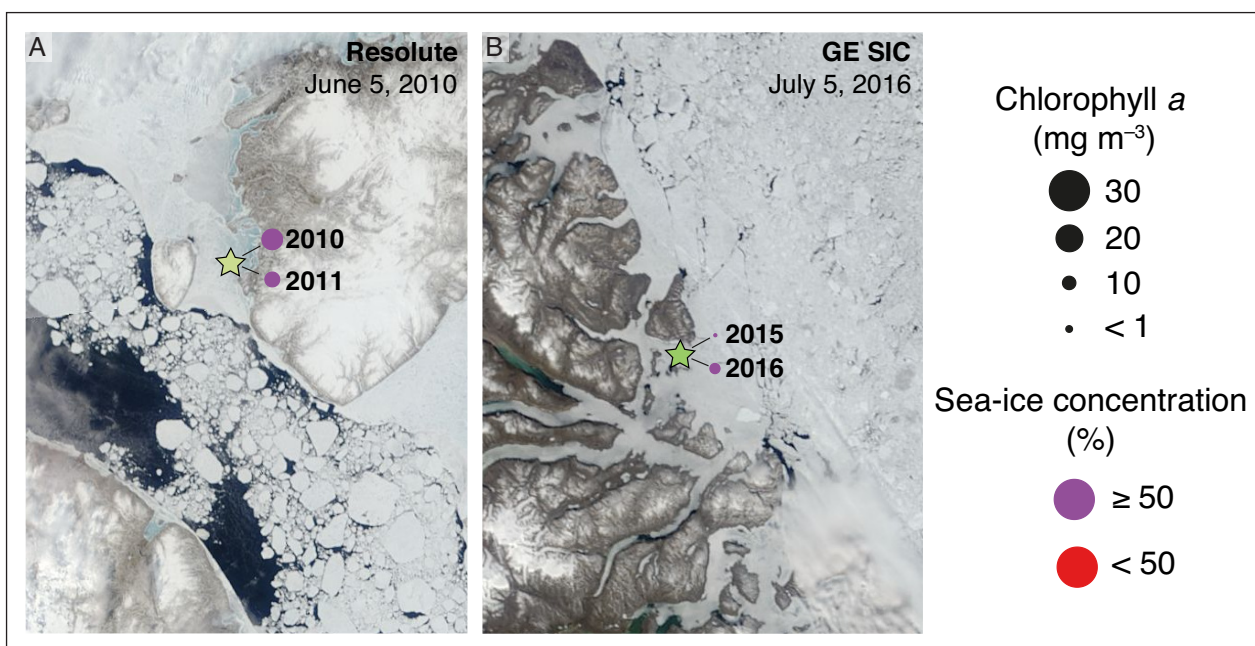


Figure 3: Terra MODIS satellite images showing locations of the sea-ice camps. The date of the image was at the peak of the phytoplankton bloom (maximum chl *a* concentration, as depicted by the size of the dots; mg m^{-3}) in 2010 for Resolute and 2016 for Green Edge. Red and purple indicate sea-ice concentration on the date of the sampling, $<50\%$ and $\geq 50\%$, respectively. DOI: <https://doi.org/10.1525/elementa.430.f3>

between Pacific waters to the west and Atlantic waters to the east (**Figure 5A**; see also Randelhoff et al., 2019). Finally, the sea-ice camps were dominated by Arctic waters of Pacific origin. Main water masses were identified based on their hydrographic and nutrient (ANP) signatures. Atlantic waters were characterized by low (~ 0) ANP values and are warm and saline (conservative temperature $T_c > 0^\circ\text{C}$, and absolute salinity $S_A > 34.0 \text{ g kg}^{-1}$; **Figure 5C**).

Winter Atlantic waters and Atlantic cold halocline waters are saline waters from the Atlantic which have cooled down during the previous winter ($T_c < 0^\circ\text{C}$, and $S_A > 33.0 \text{ g kg}^{-1}$; **Figure 5C**). They are generally located below the Atlantic or Arctic waters (less buoyant) and have different salinity in the Atlantic sector (N-ICE, $S_A \sim 34.5 \text{ g kg}^{-1}$) compared to Baffin Bay (GE Amundsen, $S_A \sim 33.5 \text{ g kg}^{-1}$; **Figure 5C**). The Arctic waters are fresher and colder than the Atlantic

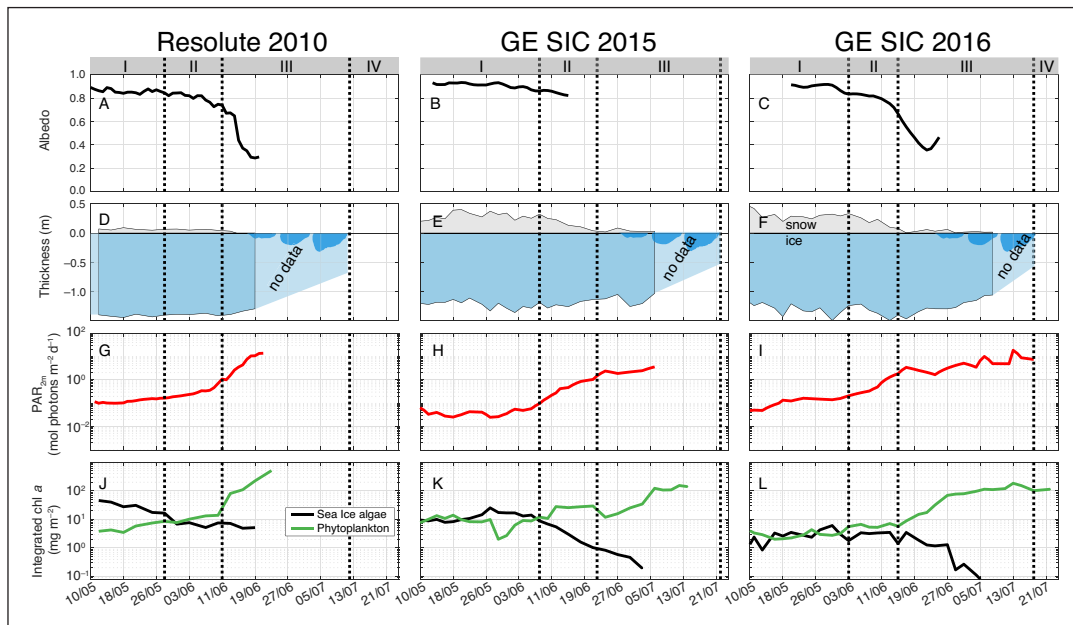


Figure 4: UIB evolution under landfast sea ice during the Resolute and Green Edge ice camps. The four main stages (I–IV) of UIB evolution are characterized by: (A–C) daily averaged *in situ* albedo; (D–F) ice and snow depth (m); (G–I) under-ice PAR at 2-m depth ($\text{mol photons m}^{-2} \text{d}^{-1}$); and (J–L) integrated chl *a* concentrations (mg m^{-2}) measured by HPLC (note the log scale) for sea-ice algae (bottom 0–3 cm of the sea ice) and phytoplankton (whole water column). Note that albedo and PAR were measured by different radiometers. See Materials and Methods and Mundy et al. (2014) and Oziel et al. (2019) for further details of data acquisition during the Resolute (2010) and Green Edge (2015 and 2016) ice camps. The four main stages are (I) the winter period, (II) the snowmelt period, (III) the melt pond period and (IV) the ice-free period, which are delimited, respectively, by snowmelt initiation, melt pond initiation, and breakup of the sea ice, as illustrated by vertical dotted lines. No data were available for sea-ice thickness (pale blue) during most of the melt pond (bright blue) period. DOI: <https://doi.org/10.1525/elementa.430.f4>

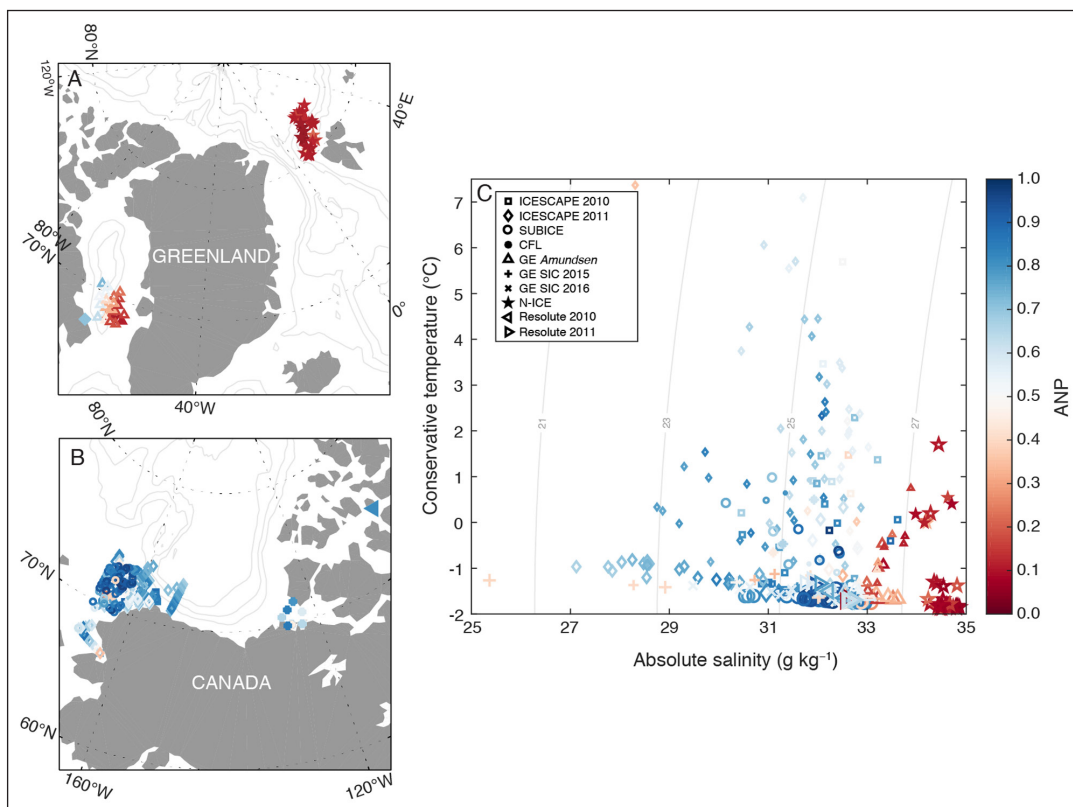


Figure 5: Atlantic- versus Pacific-derived waters sampled during the different expeditions. (A–B) Maps of the expeditions and (C) temperature–salinity diagram (conservative temperature, $^{\circ}\text{C}$; absolute salinity, g kg^{-1}) showing the “Arctic N–P relationship” (ANP) at 20-m depth. ANP values close to 0 (1) suggest a water mass signature from the Atlantic (Pacific). Isopycnals σ_{θ} are in gray lines. DOI: <https://doi.org/10.1525/elementa.430.f5>

waters ($T_c < 0^\circ\text{C}$, and $S_A < 33.0 \text{ g kg}^{-1}$) and have high (~ 1) ANP values (**Figure 5C**). The remaining points in the diagram are associated with fresh and warm surface melt waters. Their characteristics are highly scattered, but could be defined with $T_c > 0^\circ\text{C}$ and $S_A < 33.0 \text{ g kg}^{-1}$ (**Figure 5C**).

Winter nutrient concentrations were higher in Pacific-influenced coastal waters of the Western Arctic Ocean than in the sea-ice camps in the Canadian Arctic Archipelago, Arctic outflow waters of Baffin Bay, and inflowing Atlantic-influenced waters north of Svalbard (**Figure 6A–C**). In Pacific-influenced waters of the Western Arctic Ocean (e.g., SUBICE, ICESCAPE 2010 and 2011, CASES and CFL), winter water concentrations of NO_3^- , Si(OH)_4 , and PO_4^{3-} had ranges of 14.4–20.2, 31.4–64.5, and $1.64\text{--}2.5 \mu\text{mol L}^{-1}$, respectively (**Figure 6A–C**). In the sea-ice camps dominated by Arctic waters of Pacific origins (e.g., Resolute 2010 and 2011, GE SIC 2015 and 2016), winter water ranges of NO_3^- , Si(OH)_4 , and PO_4^{3-} concentrations were 6.35–10.5, 8.32–17.0, and $0.9\text{--}1.4 \mu\text{mol L}^{-1}$, respectively (**Figure 6A–C**). Finally, in Arctic outflow waters of Baffin Bay and inflowing Atlantic-influenced waters (i.e., GE Amundsen

and N-ICE), the ranges of winter water NO_3^- , Si(OH)_4 , and PO_4^{3-} concentrations were 12.2–12.9, 3.42–12.8, and $0.9\text{--}1.21 \mu\text{mol L}^{-1}$, respectively (i.e., GE Amundsen and N-ICE; **Figure 6A–C**).

By spring, nutrient drawdown was generally high in the western Arctic (Chukchi Sea), with the two ICESCAPE expeditions having the greatest drawdown of Si(OH)_4 (47.0 and $59.0 \mu\text{mol L}^{-1}$) and PO_4^{3-} ($\sim 2.1 \mu\text{mol L}^{-1}$) (**Figure 7A–C**). The lowest Si(OH)_4 drawdown ($3.0\text{--}4.0 \mu\text{mol L}^{-1}$) was seen in the Resolute 2010, GE SIC 2015 and 2016, and N-ICE expeditions. Similarly, PO_4^{3-} drawdown ($0.2\text{--}0.4 \mu\text{mol L}^{-1}$) was lowest in the Resolute 2010 and both GE SIC studies. Drawdown of NO_3^- was also high (14.4 and $20.2 \mu\text{mol L}^{-1}$) at the ICESCAPE sites but similar to drawdown during the CFL expedition. NO_3^- drawdown was slightly less (11.7 and $12.9 \mu\text{mol L}^{-1}$) in the N-ICE and GE Amundsen studies, and much less ($2.5\text{--}5.0 \mu\text{mol L}^{-1}$) in the Resolute and GE SIC studies. Although the SUBICE and ICESCAPE studies were both in the Chukchi Sea, SUBICE took place earlier in the season (**Figure 1**) when the bloom did not deplete nutrient inventories, particularly PO_4^{3-} and Si(OH)_4 , to the same extent.

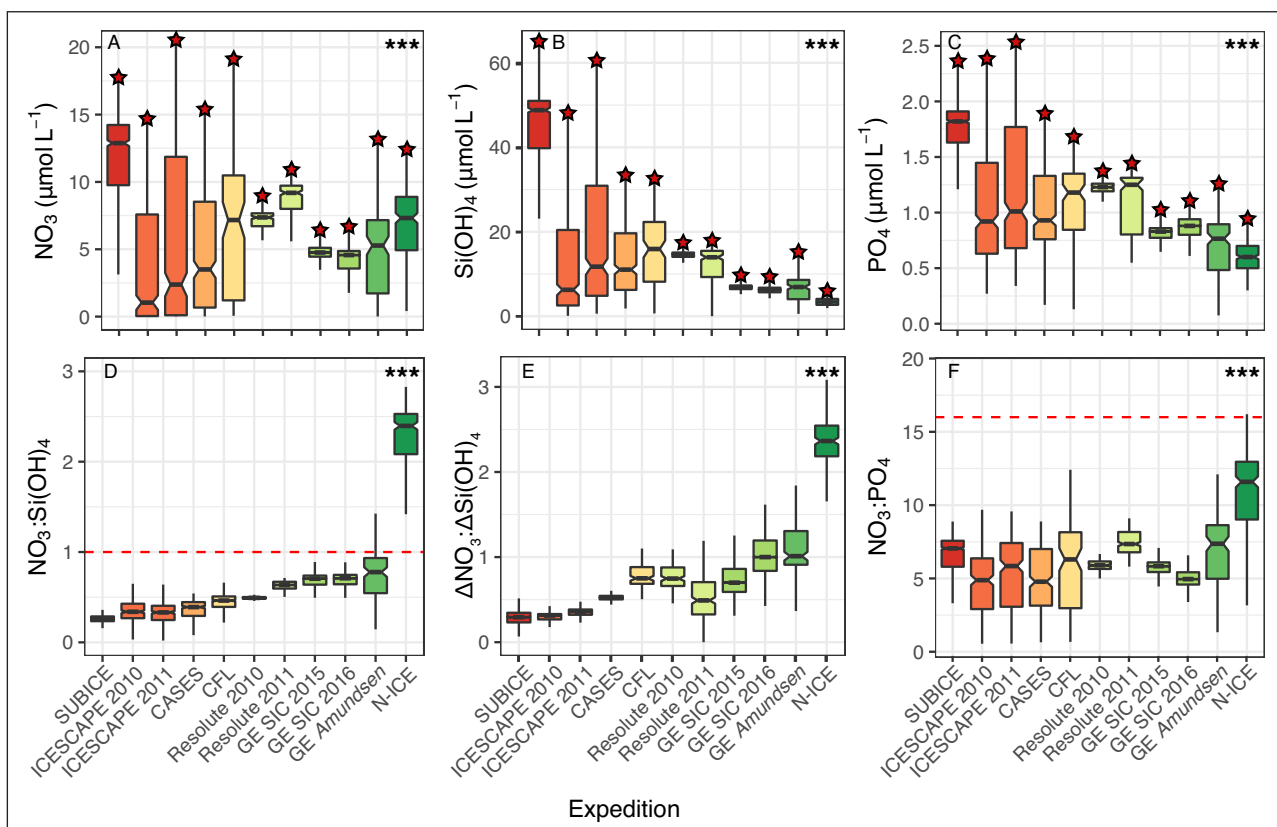


Figure 6: Nutrient concentrations and ratios of the different expeditions. Box plots for the different expeditions showing water column concentrations of (A) nitrate (NO_3^-), (B) silicate (Si(OH)_4), and (C) phosphate (PO_4^{3-}), and the ratios (D) $\text{NO}_3^-:\text{Si(OH)}_4$, (E) $\Delta\text{NO}_3^-:\Delta\text{Si(OH)}_4$ and (F) $\text{NO}_3^-:\text{PO}_4^{3-}$. The line in the middle of each box represents the median; the top and bottom limits are the 25th and 75th percentiles, respectively. The lines extending above and below each box (whiskers) represent the full range of non-outlier observations for each variable beyond the quartile range. The results of the Kruskal-Wallis H test depict regions with statistically significant differences at the 95% confidence level ($p < 0.05$). The codes of the significance test are *: $p < 0.01$, **: $p < 0.001$ and ***: $p < 0.0001$. The red stars show the maximum value in nutrient concentration (i.e., NO_3^- , Si(OH)_4 , PO_4^{3-}) for the different expeditions. The dashed red lines indicate the Redfield ratios for (D) N:Si and (F) N:P. DOI: <https://doi.org/10.1525/elementa.430.f6>

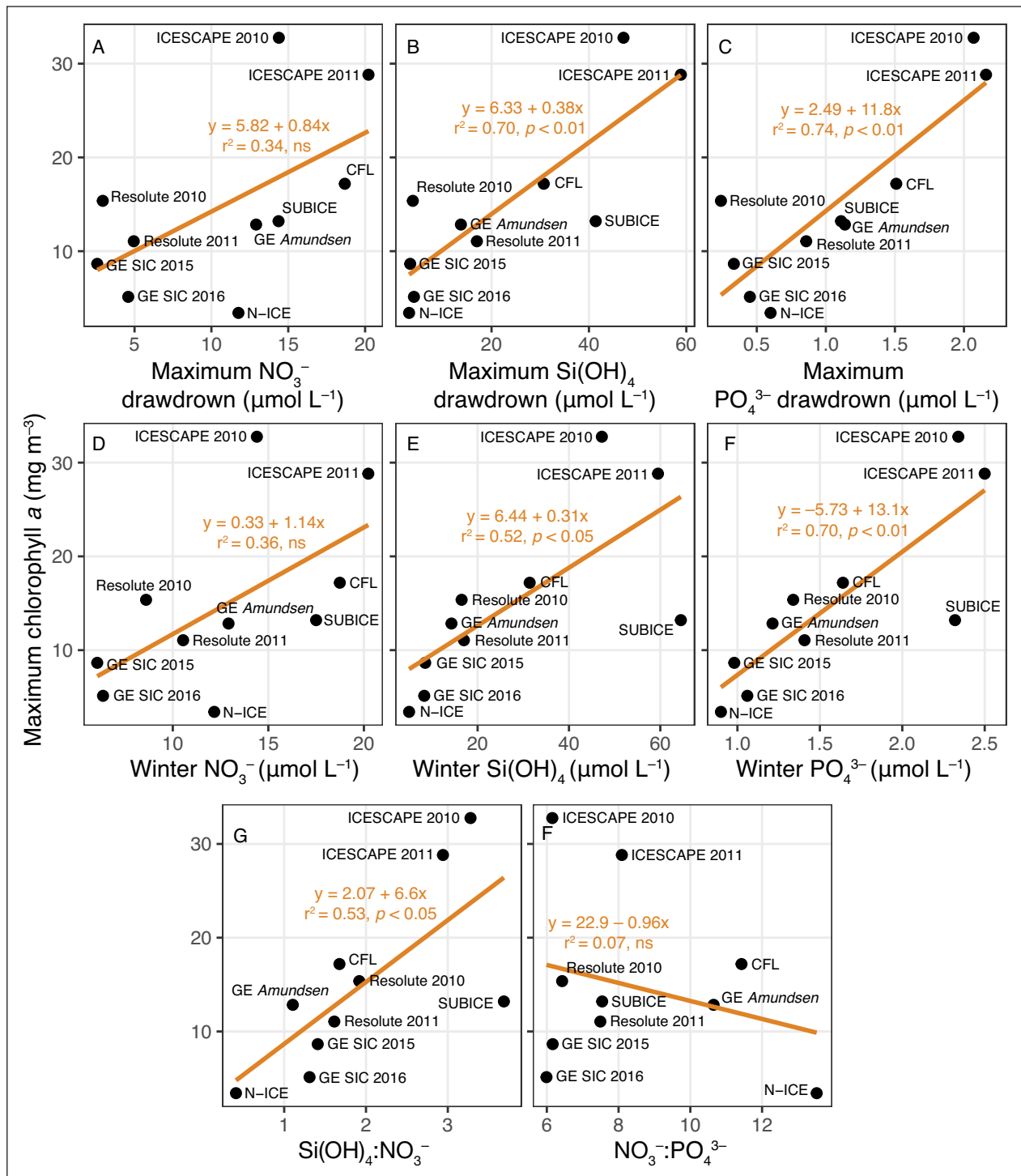


Figure 7: Relationships between under-ice bloom magnitude and nutrient drawdown, winter nutrient concentrations and winter nutrient ratios. UIB magnitude, represented by the maximum measured chl *a* concentration for each expedition, is plotted against (A–C) nutrient drawdown, (D–F) winter water nutrient concentration, and (G, H) winter water nutrient ratios. Lines indicate best fits determined using least squared linear regression, with both the coefficient of determination (r^2) and statistical significance of the goodness of fit test ($\alpha < 0.05$) presented; ns indicates not significant. DOI: <https://doi.org/10.1525/elementa.430.f7>

3.2. Biomass and diversity of phytoplankton blooms

Based on our pan-Arctic compilation, a diverse array of phytoplankton blooms, reported in contrasting sea-ice conditions, varied considerably in terms of magnitude and structure (Figures 2, 3, 8 and 9). The maximum chl *a* concentrations of the UIBs ranged from massive diatom blooms in the Chukchi Sea (e.g., 30.0 mg

chl *a* m⁻³; Figures 2A, B and 8A, B) to modest UIBs north of Svalbard (e.g., 3.41 mg chl *a* m⁻³; Figures 2D and 8J). In some cases, the maximum values of chl *a* concentration associated with the UIBs were similar to those in adjacent sea-ice-free conditions (e.g., 32.8 mg chl *a* m⁻³ in the Chukchi Sea; Figures 2A, B and 8A, B). The bloom magnitude decreased from the western to the eastern Arctic

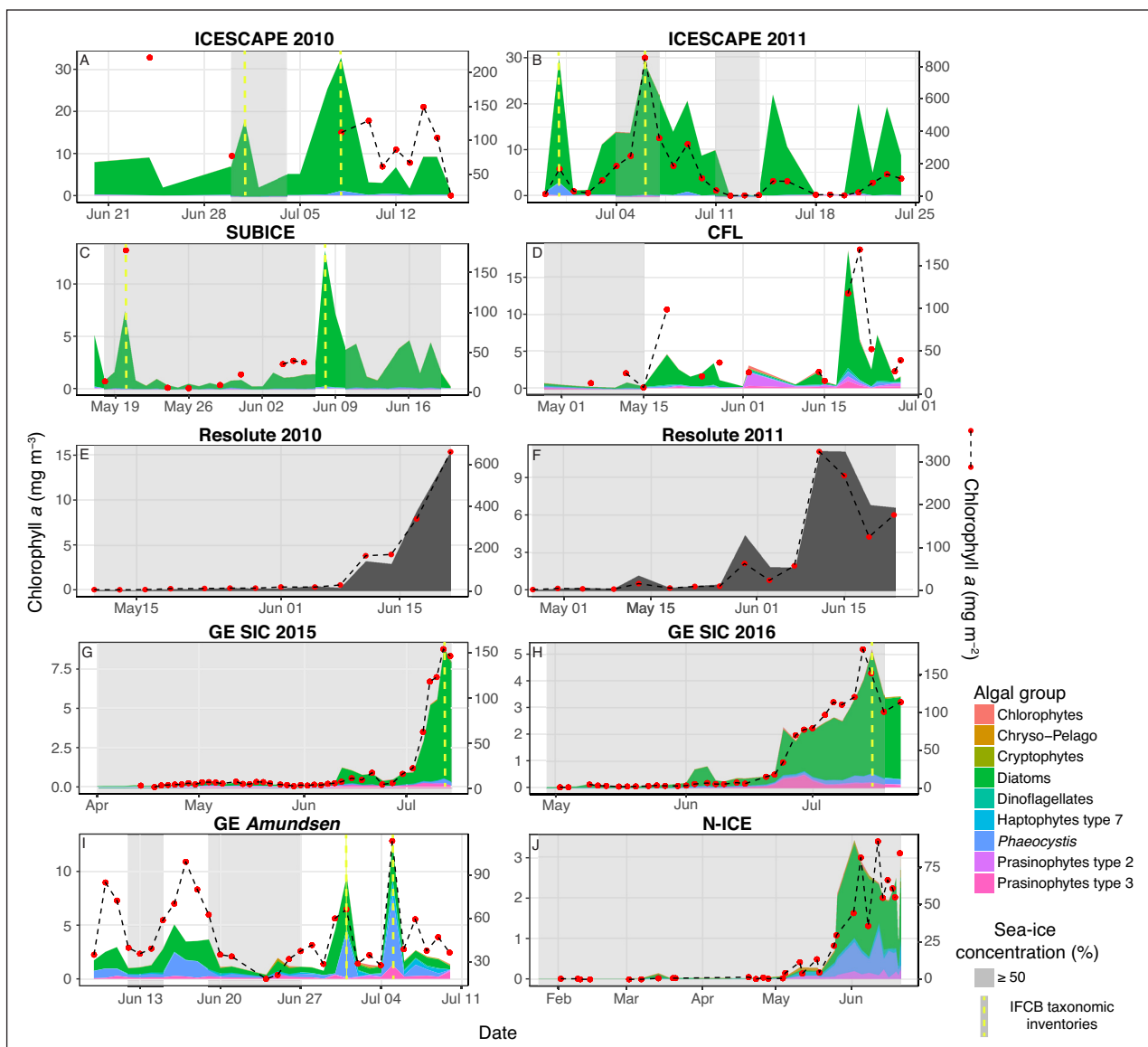


Figure 8: Temporal succession of the major algal groups. CHEMTAX was used at the depth of the maximum chl a concentration (as indicated in mg m^{-3}) in the upper water column (**A–I**) for different expeditions. The different algal groups considered are: chlorophytes, chryso-pelagophytes, cryptophytes, diatoms, dinoflagellates, haptophytes type 7, *Phaeocystis*, prasinophytes type 2, and prasinophytes type 3. The depth-integrated chl a biomass over the first 100 meters (in mg m^{-2}) is shown by the red dots connected by dashed lines. Gray boxes indicate sea-ice concentration $\geq 50\%$. Vertical yellow dashed lines show stations for which IFCB taxonomic data were also analyzed. Note that for Resolute 2010 and 2011, only the chl a concentration at the depth of the SCM is shown (not by taxonomic groupings) in dark gray. DOI: <https://doi.org/10.1525/elementa.430.f8>

Ocean (i.e., $30.0 \text{ mg chl } a \text{ m}^{-3}$ in the Chukchi Sea, $17.2 \text{ mg chl } a \text{ m}^{-3}$ in the Beaufort Sea/Amundsen Gulf, $15.4 \text{ mg chl } a \text{ m}^{-3}$ in the Canadian Arctic Archipelago, and $12.8 \text{ mg chl } a \text{ m}^{-3}$ in Baffin Bay; **Figures 2, 3 and 8**), with some exceptions to this general trend. First, the maximum chl a concentration (mg m^{-3}) and depth-integrated chl a (mg m^{-2}) over the first 100 meters are highly correlated ($r^2 = 0.71$, $p < 0.0001$; **Figure 8**), though differences between the two can be large when subsurface chl a maxima (SCMs) are present in open water. Second, the higher bloom magnitude observed in the Beaufort Sea/Amundsen Gulf (CFL cruise; **Figures 2F and 8D**) was associated with a localized ice-edge upwelling event (Mundy et al., 2009). These observations are not common for the Beaufort Sea, which

is classified more typically as an oligotrophic system with N-depleted stratified surface waters (Tremblay et al. 2008; Brugel et al. 2009; Ardyna et al. 2017).

The maximum chl a concentration measured during each bloom was related to maximum macronutrient drawdown (**Figure 7A–C**), but, surprisingly, NO_3^- drawdown was not a good predictor of this measure of bloom magnitude ($r^2 = 0.34$, $p = 0.08$). Instead, Si(OH)_4 ($r^2 = 0.70$, $p < 0.01$) and PO_4^{3-} ($r^2 = 0.74$, $p < 0.01$) drawdown were both significantly positively correlated to the measured maximum chl a concentration. Similarly, both winter water Si(OH)_4 ($r^2 = 0.52$, $p < 0.05$) and PO_4^{3-} ($r^2 = 0.70$, $p < 0.01$) concentrations were significantly correlated to maximum measured chl a concentrations, while winter

water NO_3^- ($r^2 = 0.36$, $p = 0.07$) concentration was not (Figure 7D–F). The ratio $\text{Si(OH)}_4:\text{NO}_3^-$ of the winter water across the different sites was also a significant predictor of the maximum measured chl a ($r^2 = 0.53$, $p < 0.05$; Figure 7G). The highest chl a concentrations measured across all sites were in regions that had the highest concentrations of winter water Si(OH)_4 . In fact, the four campaigns that had Si(OH)_4 concentrations $>30 \mu\text{mol L}^{-1}$ (SUBICE, ICESCAPE 2010 and 2011, and CFL) averaged 2.4x higher chl a concentrations than the other sites. Si(OH)_4 was 4.4x higher at these four sites while NO_3^- and PO_4^{3-} were only 1.9x higher. Predictably, the blooms at the sites with the greatest Si(OH)_4 concentrations were dominated fractionally to the greatest extent by diatoms (see below).

UIBs are typically dominated by diatoms, as both CHEMTAX and the IFCB images reveal (Figures 8 and 9). Several genera of the dominant diatoms in UIBs have been identified, including *Chaetoceros*, *Thalassiosira*, and *Fragilariopsis* in the Chukchi Sea during ICESCAPE (where diatoms summed to 75% and 96% of the biovolume in 2010 and 2011, respectively; Figure 9) and SUBICE (where they summed 98% of the biovolume; Figure 9). In the eastern Arctic Ocean, the decrease in the UIB magnitude was associated with a diminishing

contribution by diatoms and an increase in *Phaeocystis* (Figure 8). High abundance of *Phaeocystis pouchetii* was observed in Baffin Bay during the GE *Amundsen* cruise (up to 65% of the biovolume in open waters; Figure 9) and north of Svalbard in sea-ice-covered waters during N-ICE (Figure 8J). During the Green Edge sea-ice camps, diatoms remained dominant during the UIB periods, again with *Chaetoceros* and *Thalassiosira* as the most abundant genera (from 97% to 86% of the biovolume in 2015 and 2016, respectively). Based on CHEMTAX, a modest abundance of prasinophyte type 3 was observed during three expeditions (i.e., CFL, Green Edge sea-ice camp 2016, and GE *Amundsen* cruise; Figure 8D, H, I), which was likely the endemic Arctic prasinophyte *Micromonas polaris* (previously called *Micromonas pusilla*; Simon et al., 2017; Joli et al., 2018).

3.3. Critical factors shaping bloom magnitude and assemblages

After considering numerous environmental factors (listed in Figure 10), nutrient concentrations were shown to be the critical drivers explaining variability in phytoplankton bloom magnitude and assemblage composition (Figures 7 and 10). Based on CHEMTAX, only the relative

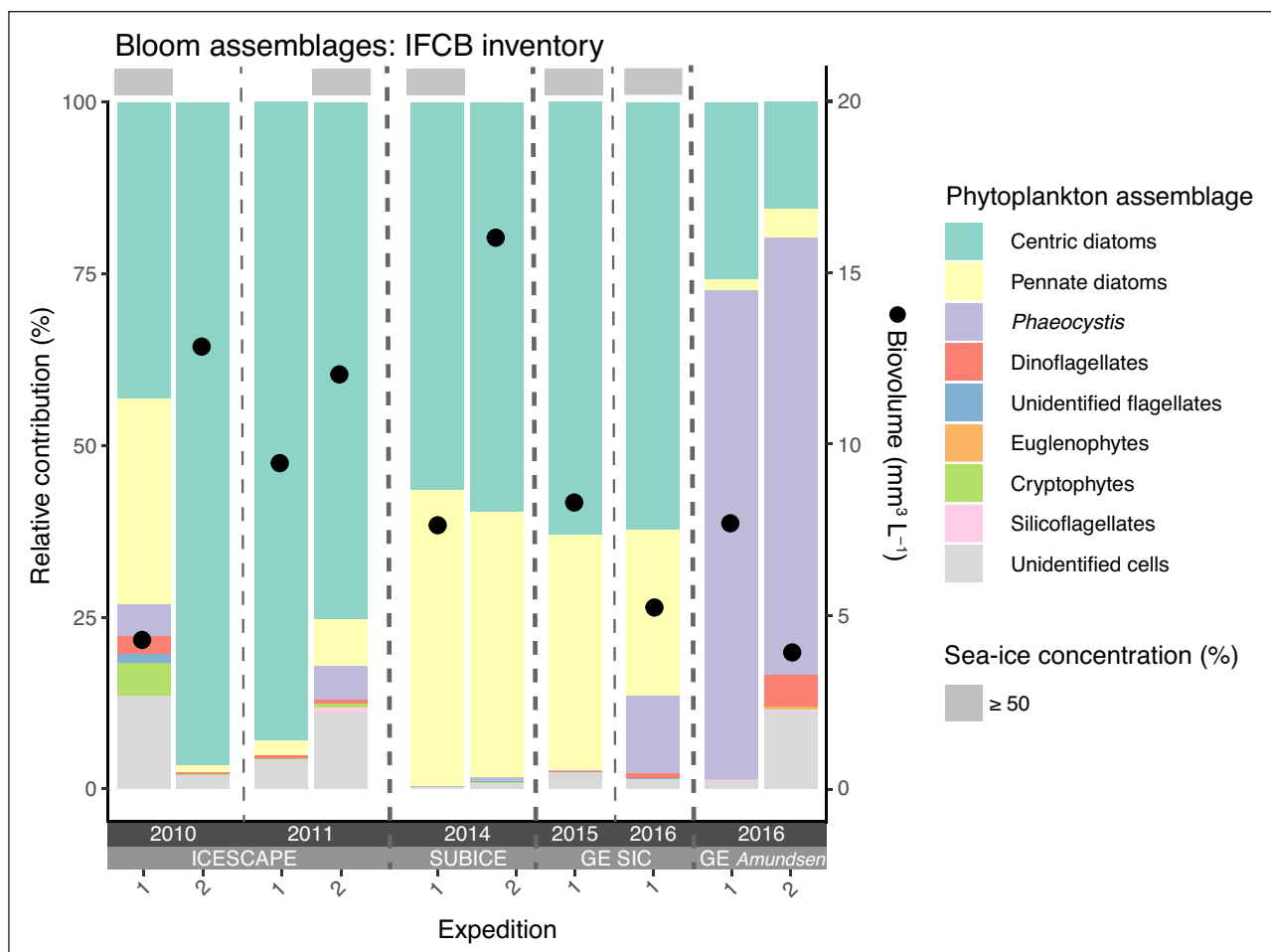


Figure 9: Relative and absolute contributions to UIB biovolume by phytoplankton groups for the different expeditions. The IFCB taxonomic data were analyzed at the peak of the blooms (as indicated by the yellow dashed lines in Figure 6). Gray boxes across the top indicate sea-ice concentration $\geq 50\%$. DOI: <https://doi.org/10.1525/elementa.430.f9>

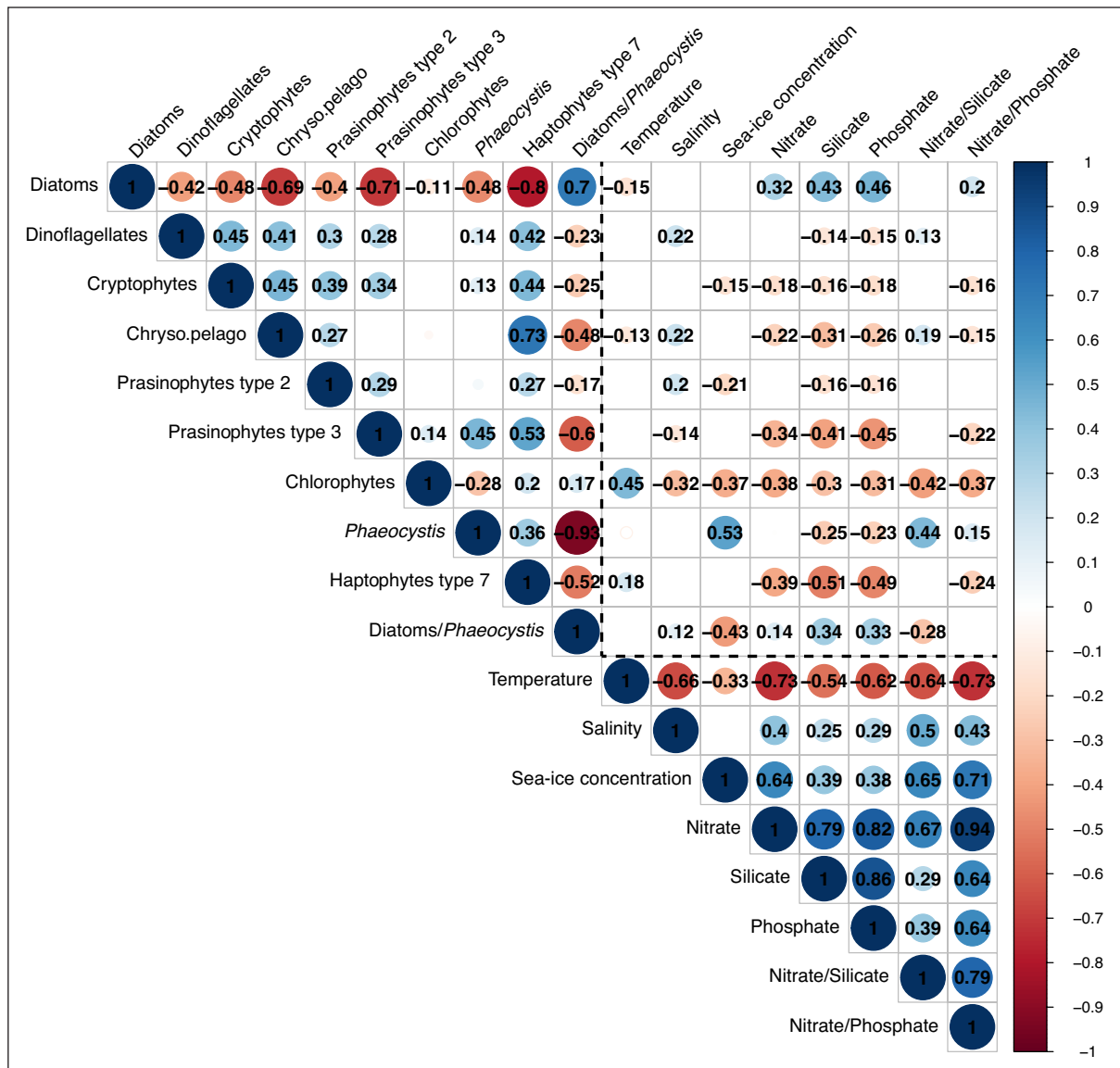


Figure 10: Heat map of the correlation coefficients between the major algal groups and environmental drivers. The correlation matrix is based on all cruise and sea-ice camp expeditions. Only significant coefficients (based on Spearman’s ρ) and absolute correlation coefficients (if >0.10) are indicated. The size of a circle indicates the absolute correlation coefficient. DOI: <https://doi.org/10.1525/elementa.430.f10>

abundance of diatoms correlated positively with nutrient concentrations (Figure 10). All of the remaining phytoplankton groups correlated negatively with Si(OH)_4 and PO_4^{3-} and most also correlated negatively with NO_3^- (with the exception of dinoflagellates, prasinophytes type 2 and *Phaeocystis*). When these negative correlations were strongly significant (as for chlorophytes, haptophytes type 7, prasinophytes type 3), nutrient concentrations were very low and/or sampling was conducted during post-bloom periods.

The molar ratio $\text{NO}_3^-:\text{Si(OH)}_4$ correlated positively with the relative abundance of *Phaeocystis* and thus negatively with the relative abundance ratio of diatoms to *Phaeocystis*, suggesting that Si(OH)_4 availability plays a critical role in controlling the relative abundance of the two main bloom-forming phytoplankton groups. $\text{NO}_3^-:\text{Si(OH)}_4$ molar ratios of <1 tended to favor diatom-dominated UIBs, while *Phaeocystis* seems to play a co-dominant

role in Atlantic-influenced waters with $\text{NO}_3^-:\text{Si(OH)}_4$ molar ratios >1 , as observed to some extent in Baffin Bay and north of Svalbard (Figure 6D). Finally, the $\text{NO}_3^-:\text{PO}_4^{3-}$ molar ratio was low across all the expeditions, with values <7.5 for all studies except N-ICE, which had a $\text{NO}_3^-:\text{PO}_4^{3-}$ of 11.6 (Figure 6F).

A strong positive correlation was observed for *Phaeocystis* and sea-ice concentration (Figure 10), indicating that factors other than nutrient concentrations and ratios could play a critical role in shaping UIB composition. The most likely factor, modulated by sea-ice concentration (including algal blooms in the ice) and snow cover, is the under-ice light field.

4. Discussion

An important and unresolved question about UIBs still remains: are they really new phenological characteristics or have they simply not been recognized historically and

integrated into Arctic phytoplankton paradigms? The re-examination of datasets from previous expeditions over the past two decades suggests that UIBs may have already had a circumpolar distribution. High concentrations of phytoplankton biomass under Arctic sea ice (typically with >50% coverage) have been reported in areas as widespread as Resolute Passage and Allen Bay in the Canadian Arctic Archipelago (Michel et al., 1996; Fortier et al., 2002; Duerksen et al., 2014; Galindo et al., 2014, 2015, 2016; Mundy et al., 2014), Baffin Bay (Hussherr et al., 2017; Oziel et al., 2019), the Greenland Sea (Mayot et al., 2018), the Barents Sea (Strass and Nöthig, 1996; Assmy et al., 2017; Pavlov et al., 2017; Kauko et al., 2019), the Laptev Sea (Lalande et al., 2014), the Chukchi Sea (Yager et al., 2001; Arrigo et al., 2012, 2014; Ha et al., 2015; Hill et al., 2018), and the Central Arctic (Laney et al., 2014; Boles et al., 2020). Many locations where UIBs were observed had first year sea ice, which was not the case in the 1980s when multi-year sea-ice was more prevalent (Figure 11). In the Arctic Ocean, the first-year ice comprised 61% of the total sea-ice coverage in March 2018 (i.e., an area of 3.2×10^6 km²), but only 34% in March 1984 (Figure 11; Tschudi et al., 2019). Such a radical transformation of the icescape, with the loss of multi-year sea ice and an overall sea-ice thinning, has certainly contributed to the greater exploration of the Arctic Ocean and the more regular observation of UIBs throughout it. Given this context, a pan-Arctic compilation of comparable data sets on UIBs provides an important opportunity to gain a more comprehensive understanding of the environmental and ecological processes underlying UIB initiation, magnitude, and phytoplankton assemblages.

4.1. Changing icescape drives phytoplankton dynamics and under-ice blooms

Sea-ice edge blooms (as observed in Figure 2) are known to begin once the highly reflective sea-ice retreats in spring, as solar elevation increases, and surface waters become stratified by the addition of sea-ice melt water. With a more fragmented and thinner sea-ice environment, however, UIBs are expected to increase throughout the Arctic Ocean (e.g., in the Chukchi Sea, the Canadian High Arctic and north of Svalbard; Figures 2 and 3) due to increasing under-ice light that drives bloom initiation. By combining three distinctive times series (i.e., the Resolute and Green Edge sea-ice camps), we propose here a conceptual representation (potentially generalizable to first-year sea ice AO areas) of the main physical drivers of under-ice light availability and, ultimately, the initiation of UIBs. For this representation, only the expeditions that were considered to be “pseudo-eulerian” and where biomass was produced locally were selected (i.e., the ice camps). Unfortunately, these criteria were not met by the expeditions, such as ICESCAPE 2011, where the massive UIB, given its magnitude and the high dominance by centric diatoms (Figures 2, 8 and 9), certainly started several weeks prior to sampling. Even with these constraints, we were able to delineate similar temporal patterns with four successive stages and three structuring events of UIB dynamics, driven mostly by changing snow, sea-ice conditions, and under-ice light availability (Figure 4):

Stage I: This first stage is defined by winter snow and ice conditions with a relatively constant high albedo (>0.85), low under-ice PAR (<0.1–0.2 mol

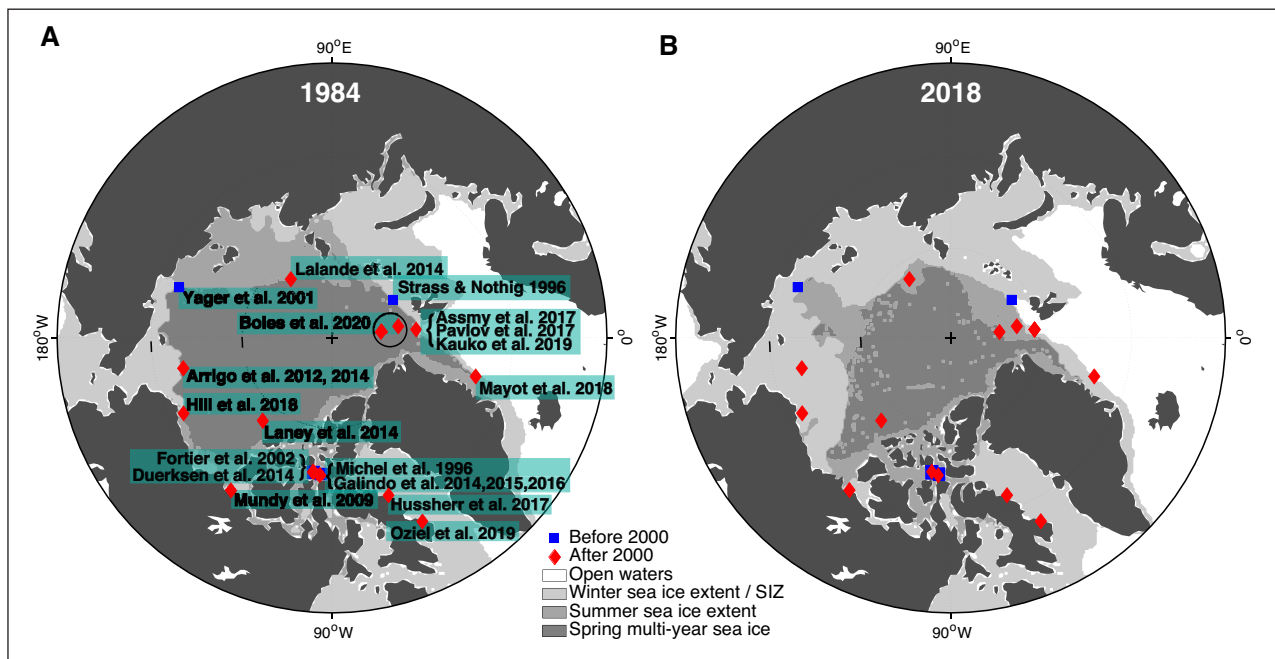


Figure 11: Pan-Arctic distribution of documented UIBs. Sea-ice maps of the Arctic Ocean are shown for (A) 1984 and (B) 2018, where white indicates open ocean; light gray, winter sea-ice extent (i.e., March); gray, summer sea-ice extent (i.e., September); and dark gray, winter multi-year (i.e., March) sea ice. Blue squares and red diamonds respectively indicate expeditions before 2000 and after 2000. See Figure 1 for the months when each expedition took place. DOI: <https://doi.org/10.1525/elementa.430.f11>

photons $\text{m}^{-2} \text{d}^{-1}$), and the development of a sea-ice algal bloom.

Stage II: This second stage is triggered by the onset of snow melt, which decreases the albedo (<0.85), increases under-ice PAR ($>0.1\text{--}0.2$ mol photons $\text{m}^{-2} \text{d}^{-1}$), and marks the concomitant termination of the sea-ice algal bloom and the initiation of the UIB. Stage II lasts approximately two weeks.

Stage III: This third stage is characterized by the appearance of melt ponds. Albedo decreases (<0.75), under-ice PAR rapidly increases ($\sim 1\text{--}2$ mol photons $\text{m}^{-2} \text{d}^{-1}$) and the UIB reaches its maximum in terms of depth-integrated biomass. Peak biomass is controlled by the balance between euphotic zone depth and surface nutrient inventories (Oziel et al., 2019). Stage III ends when the sea-ice breaks up.

Stage IV: This last stage consists of the transition to an ice-free ocean (albedo <0.2) and the deepening of phytoplankton biomass to form a subsurface chl *a* maximum at the depth where the balance between light and nutrient availability is still sufficient for phytoplankton growth. The duration of phase IV depends on the depth of the nitracline (i.e., generally related to the upper halocline) and the nutrient inventories in the halocline down to the base of the euphotic zone (Tremblay et al., 2008; Bergeron et al., 2014).

4.2. Changing nutriscaples and icescaples shape phytoplankton assemblages

Based on this novel pan-Arctic compilation, two main types of Arctic phytoplankton blooms were identified (occurring under both sea-ice-covered and sea-ice-free conditions; **Figure 8**), those dominated by diatoms and those dominated by the haptophyte *Phaeocystis pouchetii* (**Figures 8 and 9**). *Phaeocystis pouchetii* blooms have long been observed in the European Arctic sector (Smith et al., 1991; Schoemann et al., 2005) but have only recently been observed in Labrador fjords (Simo-Matchim et al., 2017) and Baffin Bay. Amongst these blooms, only one has been designated as an UIB (Assmy et al., 2017). NO_3^- is generally the main limiting nutrient in Arctic waters (Harrison and Cota, 1991), driving shifts from diatom- to flagellate-based assemblages as NO_3^- is depleted (Ardyna et al., 2011). We suspect that high NO_3^- and low Si(OH)_4 waters, i.e., having a $\text{NO}_3^-:\text{Si(OH)}_4$ molar ratios >1 (as previously suggested for open waters by Brzezinski, 1985; Legendre et al., 1993; Takeda, 1998; and Krause et al., 2018), could also drive assemblage shifts from diatom to *Phaeocystis* dominance in sea-ice-covered areas. During an expedition to Svalbard fjords and the Barents Sea in May 2016, Krause et al. (2018) demonstrated that depleted Si(OH)_4 concentrations during the peak or late phase of the spring bloom drastically reduced Si(OH)_4 uptake rates and limited diatom growth. Depending on the severity of the Si(OH)_4 limitation, more favorable growth conditions for *Phaeocystis* compared to diatoms (Nöthig et al., 2015) could result in succession from diatoms to *Phaeocystis* (i.e., only if Si(OH)_4 is exhausted before NO_3^-). Since the early 1990s, Si(OH)_4

concentrations have been declining in the North Atlantic Ocean (Rey, 2012) due to natural multi-decadal variability through a decrease in the maximal depth of winter convection and weakening of the subpolar gyre (Hátún et al., 2017). This low and declining Si(OH)_4 inventory sets a lower limit to the build-up of diatom biomass relative to what is possible in the Pacific sector, leaving NO_3^- for non-diatom phytoplankton (*Phaeocystis*) to utilize. As a result, more evidence may be found of increasing high NO_3^- and low Si(OH)_4 waters where *Phaeocystis* accounts for a relatively large share of the seasonal NO_3^- consumption, for example in Baffin Bay (influenced directly by Atlantic waters in the eastern AO; **Figure 4**) and in higher latitude waters of the European Arctic sector.

Additionally, our analysis identifies Si(OH)_4 and PO_4^{3-} , rather than NO_3^- , as good predictors of UIB magnitude (i.e., maximum chl *a*; **Figure 7**). Winter water concentrations of both nutrients, as well as their maximum drawdown, were significantly related to the maximum chl *a* measured at each study site. Likewise, those campaigns that had winter water concentrations of $\text{Si(OH)}_4 > 30 \mu\text{mol L}^{-1}$ averaged maximum chl *a* concentrations 2.4x higher than campaigns with lower Si(OH)_4 concentrations. Three of these high Si(OH)_4 campaigns (ICESCAPE 2010 and 2011 and SUBICE) recorded diatoms as $>75\%$ of the phytoplankton community (no assemblage information available from the fourth campaign, CFL). These three campaigns recorded the lowest $\text{NO}_3^-:\text{Si(OH)}_4$ drawdown ratios (mean of 0.26 ± 0.04), as well as low $\text{NO}_3^-:\text{PO}_4^{3-}$ drawdown ratios (mean of 7.05 ± 1.08 ; **Figure 6D, F**). As such, blooming diatoms use less NO_3^- per unit of Si(OH)_4 or PO_4^{3-} used. Given that the C:N between different phytoplankton varies much less than either C:Si or C:P, diatoms can likely grow to greater biomass on the same N inventory than other taxa, and thus both winter water Si(OH)_4 and PO_4^{3-} concentrations, and $\text{Si(OH)}_4:\text{NO}_3^-$ and $\text{NO}_3^-:\text{PO}_4^{3-}$ drawdown ratios, are good predictors of bloom magnitude. That maximum chl *a* was predicted best by Si(OH)_4 and PO_4^{3-} is surprising, given that NO_3^- is generally considered the nutrient that limits Arctic phytoplankton growth (Tremblay and Gagnon, 2009; Ardyna et al., 2011; Mills et al., 2018; Randelhoff et al., 2020). We suspect that, while NO_3^- is typically the first nutrient depleted during typical Arctic UIBs, the inventory of nutrients (specifically Si(OH)_4) allows for the growth of diatoms which can attain higher biomass than other taxa on the same inventory of NO_3^- .

Despite the observed Si(OH)_4 decline in the Atlantic inflow to the Arctic Ocean over the last 25 years, diatoms play a significant role for the phytoplankton spring bloom in the Atlantic sector of the Arctic (Johnsen et al., 2018; Krause et al., 2018), and relative low winter Si(OH)_4 concentrations of $4\text{--}5 \mu\text{mol L}^{-1}$ are not limiting at the start of the growth season (Mousing et al., 2018). During N-ICE, Si(OH)_4 concentrations remained at winter values of around $4 \mu\text{mol L}^{-1}$ throughout the UIB, except for a few days in early June when the UIB was dominated by a mixed diatom-*Phaeocystis* community and Si(OH)_4 concentrations were $<3 \mu\text{mol L}^{-1}$ (Assmy et al., 2017). Thus, the low but variable light field under the consolidated,

snow-covered ice pack with leads was hypothesized to favor *Phaeocystis* over diatoms during N-ICE (Assmy et al., 2017), as the former seems to be better adapted to those light conditions (as observed in the Southern Ocean; Arrigo et al., 1999, 2010). Indeed, the typical spring bloom diatoms were present at low abundances during N-ICE but did not increase to considerable biomass, except in the snow-infiltration layers which presumably had higher and more constant light levels (Fernandez-Mendez et al., 2018). High light acclimation of large diatoms dominating an apparent UIB north of Svalbard indicated that the bloom had instead developed in open waters and subsequently advected beneath the snow-covered sea ice (Johnsen et al., 2018), emphasizing the importance of the under-ice light field in determining UIB composition. Diatom-dominated UIBs considered in this study were generally observed during the melt season characterized by extensive melt pond coverage and hence under a more transparent sea-ice cover (i.e., Arrigo et al., 2012, 2014; Mundy et al., 2014; Oziel et al., 2019; see also **Figure 4**).

4.3. Changes in phytoplankton assemblages drive carbon transfer and export

As reported previously, phytoplankton biomass and assemblage structure are essential for shaping the biogeography of the Arctic Ocean (i.e., from oligotrophic to eutrophic regions; Tremblay et al., 2009; Ardyna et al., 2011). Diatom-dominated blooms both under the ice and in open water are characterized by high rates of primary production, which support a large fraction of the biomass of Arctic marine ecosystems (Tremblay et al., 2006; Ardyna et al., 2011; Arrigo et al., 2012, 2014). In contrast, shifting to a more *Phaeocystis*- and flagellated-dominated assemblage could decrease the amount of carbon transferred to higher trophic levels (Saiz et al., 2013; Ardyna et al., 2017). *Phaeocystis* blooms are generally dominated by the colony (rather than solitary) stage, which is considered unpalatable for most zooplankton grazers (Lancelot, 1995; Wilson et al., 2015; Ray et al., 2016). Although mass sedimentation of the colony stage of *Phaeocystis* blooms in the Barents Sea has been observed (Wassmann, 1994), the contribution of *Phaeocystis* to deep vertical organic carbon export is considered small compared to diatoms (Reigstad and Wassmann, 2007), unless associated with downwelling (Lalande et al., 2011), deep vertical mixing (Reigstad and Wassmann, 2007), or mineral ballast (Wollenburg et al., 2018). *Phaeocystis* tends to be mineralized in the surface water column (Wassmann, 1994). Thus, a shift towards *Phaeocystis*-dominated blooms in the European Arctic sector could weaken pelagic-benthic coupling and energy transfer to mesopelagic ecosystems.

4.4. Conclusion

Compiling and synthesizing this large data set has enabled delineation of the environmental drivers responsible for initiating and shaping the timing, magnitude, and assemblage composition of UIBs. Interestingly, both the bloom magnitude and assemblage structures in a given region were observed to be similar whether the bloom was under sea-ice cover or in open water. This similarity

implies that an increasing fraction of Arctic Ocean phytoplankton blooms could become (and potentially have been) invisible to satellite sensors, resulting in underestimates of annual net primary production by an order of magnitude or more (Arrigo et al., 2014). Early bloom formation and occurrence of UIBs have been shown to be tightly related to snow and sea-ice conditions and to the resulting under-ice light availability. In particular, a shift from multi-year to first-year sea ice (with more melt ponds and leads) could partly explain the increasing occurrence of UIBs in the Arctic Ocean (Horvat et al., 2017). Two main types of phytoplankton taxa dominate UIBs depending on the winter $\text{NO}_3^-:\text{Si}(\text{OH})_4$ ratio and the under-ice light climate. Shifts from diatom- to *Phaeocystis*-dominated blooms could occur in $\text{Si}(\text{OH})_4$ -depleted waters of the Eastern Arctic Ocean. Changes in phytoplankton assemblage composition, timing, and location could have important ramifications for Arctic biogeochemical cycles, and ultimately impact carbon flows to higher trophic levels and to the deep ocean.

Data Accessibility Statement

All data are accessible on Zenodo (DOI: <https://doi.org/10.5281/zenodo.3791608>). The taxonomic inventories (i.e., images, counts, cell characteristics) performed using the Ecotaxa application are freely available at <http://ecotaxa.obs-vlfr.fr>.

Acknowledgements

M.A. was supported by a European Union's Horizon 2020 Marie Skłodowska-Curie grant (no. 746748). This work represents a contribution to the Sorbonne Université and Stanford University. The CASES expedition was supported by a Natural Sciences and Engineering Research Council (NSERC) of Canada Network grant with logistical support from the Polar Continental Shelf Program (PCSP) of Natural Resources Canada. The CFL expedition is a contribution to the International Polar Year–Circumpolar Flaw Lead system study (IPY–CFL 2008), supported through grants from the Canadian IPY Federal program office, NSERC and numerous international collaborators. The GreenEdge project is funded by the following French and Canadian programs and agencies: ANR (Contract #111112), ArcticNet, CERC on Remote sensing of Canada's new Arctic frontier, CNES (project #131425), French Arctic Initiative, Fondation Total, CSA, LEFE and IPEV (project #1164). This project was conducted using the Canadian research icebreaker CCGS Amundsen with the support of the Amundsen Science program funded by the Canada Foundation for Innovation (CFI) Major Science Initiatives (MSI) Fund. The ICESCAPE expedition was funded by the Ocean Biology and Biogeochemistry Program and the Cryosphere Science Program of the National Aeronautic and Space Administration (NNX10AF42G to K. Arrigo, R. Pickart, and J. Swift, NNH10A0171 to D. Perovich, NNX10AT67G to W. Balch, NNX10AG36G to N. Bates and J. Mathis, NNX09AE42G and NNX11AF65G to B. G. Mitchell and C. Benitez-Nelson, NNX10AH71G to K. Frey, NNX10AG07G to S. Laney and H. Sosik, and NNX10AG05G to R. Reynolds). The N-ICE expedition was supported by the

former Centre for Ice, Climate and Ecosystems (ICE) at the Norwegian Polar Institute and the Ministry of Climate and Environment, Norway. P.A. was funded by the Research Council of Norway (project no. 244646), and the Ministry of Foreign Affairs, Norway (project ID Arctic). The Resolute expedition was supported by PCSP and by NSERC Discovery and Northern Research Supplement Grants to C.J. Mundy and M. Gosselin. The SUBICE expedition was sponsored by the NSF Office of Polar Programs (PLR-1304563 to K. R. Arrigo and PLR-1303617 to R. S. Pickart).

Competing interests

The authors have no competing interests to declare.

Author contributions

M.A. led the design of the study. M.A., M.M., L.O., P.-L. G., L.L., G.v.D. conducted the analysis. M.A., L.O., L.L. made the figures. All authors revised the earlier version of the manuscript, helped in the interpretation and approved the final version for publication.

References

- Alou-Font, E, Roy, S, Agustí, S and Gosselin, M.** 2016. Cell viability, pigments and photosynthetic performance of Arctic phytoplankton in contrasting ice-covered and open-water conditions during the spring–summer transition. *Mar Ecol Prog Ser* **542**: 89–106. DOI: <https://doi.org/10.3354/meps11562>
- AMAP.** 2017. *Snow, Water, Ice and Permafrost in the Arctic (SWIPA) 2017*. Oslo, Norway: Arctic Monitoring and Assessment Programme (AMAP).
- Anderson, LG and Macdonald, RW.** 2015. Observing the Arctic Ocean carbon cycle in a changing environment. *Polar Res* **34**(1): 26891. DOI: <https://doi.org/10.3402/polar.v34.26891>
- Antajan, E, Chrétiennot-Dinet, MJ, Leblanc, C, Daro, MH and Lancelot, C.** 2004. 19'-hexanoyloxyfucoxanthin may not be the appropriate pigment to trace occurrence and fate of *Phaeocystis*: the case of *P. globosa* in Belgian coastal waters. *J Sea Res* **52**(3): 165–177. DOI: <https://doi.org/10.1016/j.seares.2004.02.003>
- Ardyna, M, Babin, M, Devred, E, Forest, A, Gosselin, M, Raimbault, P and Tremblay, J-É.** 2017. Shelf-basin gradients shape ecological phytoplankton niches and community composition in the coastal Arctic Ocean (Beaufort Sea). *Limnol Oceanogr* **62**: 2113–2132. DOI: <https://doi.org/10.1002/lno.10554>
- Ardyna, M, Babin, M, Gosselin, M, Devred, E, Bélanger, S, Matsuoka, A and Tremblay, J-É.** 2013. Parameterization of vertical chlorophyll *a* in the Arctic Ocean: impact of the subsurface chlorophyll maximum on regional, seasonal, and annual primary production estimates. *Biogeosciences* **10**(6): 4383–4404. DOI: <https://doi.org/10.5194/bg-10-4383-2013>
- Ardyna, M, Babin, M, Gosselin, M, Devred, E, Rainville, L and Tremblay, J-É.** 2014. Recent Arctic Ocean sea-ice loss triggers novel fall phytoplankton blooms. *Geophys Res Lett* **41**(17): 6207–6212. DOI: <https://doi.org/10.1002/2014GL061047>
- Ardyna, M, Gosselin, M, Michel, C, Poulin, M and Tremblay, J-É.** 2011. Environmental forcing of phytoplankton community structure and function in the Canadian High Arctic: contrasting oligotrophic and eutrophic regions. *Mar Ecol Prog Ser* **442**: 37–57. DOI: <https://doi.org/10.3354/meps09378>
- Arndt, S and Nicolaus, M.** 2014. Seasonal cycle and long-term trend of solar energy fluxes through Arctic sea ice. *Cryosphere* **8**(3): 2219–2233. DOI: <https://doi.org/10.5194/tc-8-2219-2014>
- Arrigo, KR, Mills, MM, Dijken, GL, Lowry, KE, Pickart, RS and Schlitzer, R.** 2017. Late spring nitrate distributions beneath the ice-covered northeastern Chukchi shelf. *J Geophys Res Biogeosci* **122**(9): 2409–2417. DOI: <https://doi.org/10.1002/2017JG003881>
- Arrigo, KR, Mills, MM, Kropuenske, LR, van Dijken, GL, Alderkamp, A-C and Robinson, DH.** 2010. Photophysiology in two major Southern Ocean phytoplankton taxa: Photosynthesis and growth of *Phaeocystis antarctica* and *Fragilariopsis cylindrus* under different irradiance levels. *Integr Comp Biol* **50**(6): 950–966. DOI: <https://doi.org/10.1093/icb/icq021>
- Arrigo, KR, Perovich, DK, Pickart, RS, Brown, ZW, van Dijken, GL, Lowry, KE, Mills, MM, Palmer, MA, Balch, WM, Bahr, F, Bates, NR, Benitez-Nelson, C, Bowler, B, Brownlee, E, Ehn, JK, Frey, KE, Garley, R, Laney, SR, Lubelczyk, L, Mathis, J, Matsuoka, A, Mitchell, BG, Moore, GWK, Ortega-Retuerta, E, Pal, S, Polashenski, CM, Reynolds, RA, Schieber, B, Sosik, HM, Stephens, M and Swift, JH.** 2012. Massive phytoplankton blooms under Arctic sea ice. *Science* **336**: 1408. DOI: <https://doi.org/10.1126/science.1215065>
- Arrigo, KR, Perovich, DK, Pickart, RS, Brown, ZW, van Dijken, GL, Lowry, KE, Mills, MM, Palmer, MA, Balch, WM, Bates, NR, Benitez-Nelson, CR, Brownlee, E, Frey, KE, Laney, SR, Mathis, J, Matsuoka, A, Greg Mitchell, B, Moore, GWK, Reynolds, RA, Sosik, HM and Swift, JH.** 2014. Phytoplankton blooms beneath the sea ice in the Chukchi Sea. *Deep Sea Res Pt 2* **105**: 1–16. DOI: <https://doi.org/10.1016/j.dsr2.2014.03.018>
- Arrigo, KR, Robinson, DH, Worthen, DL, Dunbar, RB, DiTullio, GR, VanWoert, M and Lizotte, MP.** 1999. Phytoplankton community structure and the draw-down of nutrients and CO₂ in the Southern Ocean. *Science* **283**(5400): 365–367. DOI: <https://doi.org/10.1126/science.283.5400.365>
- Assmy, P, Fernández-Méndez, M, Duarte, P, Meyer, A, Randelhoff, A, Mundy, CJ, Olsen, LM, Kauko, HM, Bailey, A, Chierici, M, Cohen, L, Doulgeris, AP, Ehn, JK, Fransson, A, Gerland, S, Hop, H, Hudson, SR, Hughes, N, Itkin, P, Johnsen, G, King, JA, Koch, BP, Koenig, Z, Kwasniewski, S, Laney, SR, Nicolaus, M, Pavlov, AK, Polashenski, CM, Provost, C, Rösel, A, Sandbu, M, Spreen,**

- G, Smedsrud, LH, Sundfjord, A, Taskjelle, T, Tatarek, A, Wiktor, J, Wagner, PM, Wold, A, Steen, H and Granskog, MA.** 2017. Leads in Arctic pack ice enable early phytoplankton blooms below snow-covered sea ice. *Sci Rep* **7**: 40850. DOI: <https://doi.org/10.1038/srep40850>
- Bergeron, M and Tremblay, J-É.** 2014. Shifts in biological productivity inferred from nutrient drawdown in the southern Beaufort Sea (2003–2011) and northern Baffin Bay (1997–2011), Canadian Arctic. *Geophys Res Lett* **41**(11): 2014GL059649. DOI: <https://doi.org/10.1002/2014GL059649>
- Blais, M, Ardyna, M, Gosselin, M, Dumont, D, Bélanger, S, Tremblay, J-É, Gratton, Y, Marchese, C and Poulin, M.** 2017. Contrasting interannual changes in phytoplankton productivity and community structure in the coastal Canadian Arctic Ocean. *Limnol Oceanogr* **62**: 2480–2497. DOI: <https://doi.org/10.1002/lno.10581>
- Boles, E, Provost, C, Garçon, V, Bertosio, C, Athanase, M, Koenig, Z and Sennéchaël, N.** 2020. Under-ice phytoplankton blooms in the Central Arctic Ocean: Insights from the first biogeochemical IAOS platform drift in 2017. *J Geophys Res Oceans* **125**(3): e2019JC015608. DOI: <https://doi.org/10.1029/2019JC015608>
- Brugel, S, Nozais, C, Poulin, M, Tremblay, J-É, Miller, LA, Simpson, KG, Gratton, Y and Demers, S.** 2009. Phytoplankton biomass and production in the southeastern Beaufort Sea in autumn 2002 and 2003. *Mar Ecol Prog Ser* **377**: 63–77. DOI: <https://doi.org/10.3354/meps07808>
- Brzezinski, MA.** 1985. The Si:C:N ratio of marine diatoms: interspecific variability and the effect of some environmental variables. *J Phycol* **21**(3): 347–357. DOI: <https://doi.org/10.1111/j.0022-3646.1985.00347.x>
- Cavaliere, DJ, Parkinson, C, Gloersen, P and Zwally, HJ.** 1996. Sea ice concentrations from Nimbus-7 SMMR and DMSP SSM/I passive microwave data [1998–2007]. Boulder, Colorado USA: NASA National Snow and Ice Data Center Distributed Active Archive Center. DOI: <https://doi.org/10.5067/8GQ8LZQVLOVL>
- Coupe, P, Matsuoka, A, Ruiz-Pino, D, Gosselin, M, Marie, D, Tremblay, J-É and Babin, M.** 2015. Pigment signatures of phytoplankton communities in the Beaufort Sea. *Biogeosciences* **12**(4): 991–1006. DOI: <https://doi.org/10.5194/bg-12-991-2015>
- Duerksen, SW, Thiemann, GW, Budge, SM, Poulin, M, Niemi, A and Michel, C.** 2014. Large, omega-3 rich, pelagic diatoms under Arctic sea ice: Sources and implications for food webs. *PLoS ONE* **9**(12): e114070. DOI: <https://doi.org/10.1371/journal.pone.0114070>
- Fernández-Méndez, M, Olsen, LM, Kauko, HM, Meyer, A, Rösel, A, Merkouriadi, I, Mundy, CJ, Ehn, JK, Johansson, AM, Wagner, PM, Ervik, Å, Sorrell, BK, Duarte, P, Wold, A, Hop, H and Assmy, P.** 2018. Algal hot spots in a changing Arctic Ocean: Sea-ice ridges and the snow-ice interface. *Front Mar Sci* **5**(75). DOI: <https://doi.org/10.3389/fmars.2018.00075>
- Fortier, M, Fortier, L, Michel, C and Legendre, L.** 2002. Climatic and biological forcing of the vertical flux of biogenic particles under seasonal Arctic sea ice. *Mar Ecol Prog Ser* **225**: 1–16. DOI: <https://doi.org/10.3354/meps225001>
- Fragoso, GM, Poulton, AJ, Yashayaev, IM, Head, EJH and Purdie, DA.** 2017. Spring phytoplankton communities of the Labrador Sea (2005–2014): pigment signatures, photophysiology and elemental ratios. *Biogeosciences* **14**(5): 1235–1259. DOI: <https://doi.org/10.5194/bg-14-1235-2017>
- Galindo, V, Levasseur, M, Mundy, CJ, Gosselin, M, Scarratt, M, Papakyriakou, T, Stefels, J, Gale, MA, Tremblay, J-É and Lizotte, M.** 2016. Contrasted sensitivity of DMSP production to high light exposure in two Arctic under-ice blooms. *J Exp Mar Biol Ecol* **475**: 38–48. DOI: <https://doi.org/10.1016/j.jembe.2015.11.009>
- Galindo, V, Levasseur, M, Mundy, CJ, Gosselin, M, Tremblay, J-É, Scarratt, M, Gratton, Y, Papakiriakou, T, Poulin, M and Lizotte, M.** 2014. Biological and physical processes influencing sea ice, under-ice algae, and dimethylsulfoniopropionate during spring in the Canadian Arctic Archipelago. *J Geophys Res Oceans* **119**(6): 3746–3766. DOI: <https://doi.org/10.1002/2013JC009497>
- Galindo, V, Levasseur, M, Scarratt, M, Mundy, CJ, Gosselin, M, Kiene, RP, Gourdal, M and Lizotte, M.** 2015. Under-ice microbial dimethylsulfoniopropionate metabolism during the melt period in the Canadian Arctic Archipelago. *Mar Ecol Prog Ser* **524**: 39–53. DOI: <https://doi.org/10.3354/meps11144>
- Ha, HK, Kim, YH, Lee, HJ, Hwang, B and Joo, HM.** 2015. Under-ice measurements of suspended particulate matters using ADCP and LISST-Holo. *Ocean Sci* **50**(1): 97–108. DOI: <https://doi.org/10.1007/s12601-015-0008-2>
- Harrison, WG and Cota, GF.** 1991. Primary production in polar waters: relation to nutrient availability. *Polar Res* **10**(1): 87–104. DOI: <https://doi.org/10.1111/j.1751-8369.1991.tb00637.x>
- Hátún, H, Azetsu-Scott, K, Somavilla, R, Rey, F, Johnson, C, Mathis, M, Mikolajewicz, U, Coupe, P, Tremblay, J-É, Hartman, S, Pacariz, SV, Salter, I and Ólafsson, J.** 2017. The subpolar gyre regulates silicate concentrations in the North Atlantic. *Sci Rep* **7**(1): 14576. DOI: <https://doi.org/10.1038/s41598-017-14837-4>
- Higgins, HW, Wright, SW and Schlüter, L.** 2011. Quantitative interpretation of chemotaxonomic pigment data. In: Llewellyn, CA, Egeland, ES, Johnsen, G and Roy, S (eds.), *Phytoplankton Pigments: Characterization, Chemotaxonomy and Applications in Oceanography*, 257–313. Cambridge: Cambridge University Press. DOI: <https://doi.org/10.1017/CBO9780511732263.010>

- Hill, VJ, Light, B, Steele, M and Zimmerman, RC.** 2018. Light availability and phytoplankton growth beneath Arctic sea ice: Integrating observations and modeling. *J Geophys Res Oceans* **123**(5): 3651–3667. DOI: <https://doi.org/10.1029/2017JC013617>
- Horvat, C, Jones, DR, Iams, S, Schroeder, D, Flocco, D and Feltham, D.** 2017. The frequency and extent of sub-ice phytoplankton blooms in the Arctic Ocean. *Science Advances* **3**(3): e1601191. DOI: <https://doi.org/10.1126/sciadv.1601191>
- Hussherr, R, Levasseur, M, Lizotte, M, Tremblay, JÉ, Mol, J, Thomas, H, Gosselin, M, Starr, M, Miller, LA, Jarniková, T, Schuback, N and Mucci, A.** 2017. Impact of ocean acidification on Arctic phytoplankton blooms and dimethyl sulfide concentration under simulated ice-free and under-ice conditions. *Biogeosciences* **14**(9): 2407–2427. DOI: <https://doi.org/10.5194/bg-14-2407-2017>
- Jeffrey, SW.** 1997. Chlorophyll and carotenoid extinction coefficients. In: Jeffrey, SW, Mantoura, RFC and Wright, SW (eds.), *Phytoplankton Pigments in Oceanography*, 595–596. Paris: UNESCO Publishing.
- Johnsen, G, Norli, M, Moline, M, Robbins, I, von Quillfeldt, C, Sørensen, K, Cottier, F and Berge, J.** 2018. The advective origin of an under-ice spring bloom in the Arctic Ocean using multiple observational platforms. *Polar Biol* **41**(6): 1197–1216. DOI: <https://doi.org/10.1007/s00300-018-2278-5>
- Joli, N, Gosselin, M, Ardyna, M, Babin, M, Onda, DF, Tremblay, J-E and Lovejoy, C.** 2018. Need for focus on microbial species following ice melt and changing freshwater regimes in a Janus Arctic Gateway. *Sci Rep* **8**(1):9405. DOI: <https://doi.org/10.1038/s41598-018-27705-6>
- Kahru, M, Brotas, V, Manzano-Sarabio, M and Mitchell, BG.** 2010. Are phytoplankton blooms occurring earlier in the Arctic? *Glob Change Biol* **17**(4): 1733–1739. DOI: <https://doi.org/10.1111/j.1365-2486.2010.02312.x>
- Katlein, C, Arndt, S, Belter, HJ, Castellani, G and Nicolaus, M.** 2019. Seasonal evolution of light transmission distributions through Arctic sea ice. *J Geophys Res Oceans* **124**(8): 5418–5435. DOI: <https://doi.org/10.1029/2018JC014833>
- Kauko, HM, Pavlov, AK, Johnsen, G, Granskog, MA, Peeken, I and Assmy, P.** 2019. Photoacclimation state of an Arctic underice phytoplankton bloom. *J Geophys Res Oceans* **124**(3): 1750–1762. DOI: <https://doi.org/10.1029/2018JC014777>
- Krause, JW, Duarte, CM, Marquez, IA, Assmy, P, Fernández-Méndez, M, Wiedmann, I, Wassmann, P, Kristiansen, S and Agustí, S.** 2018. Biogenic silica production and diatom dynamics in the Svalbard region during spring. *Biogeosciences* **15**(21): 6503–6517. DOI: <https://doi.org/10.5194/bg-15-6503-2018>
- Kwok, R.** 2018. Arctic sea ice thickness, volume, and multiyear ice coverage: losses and coupled variability (1958–2018). *Environ Res Lett* **13**(10): 105005. DOI: <https://doi.org/10.1088/1748-9326/aae3ec>
- Lalande, C, Bauerfeind, E and Nöthig, EM.** 2011. Downward particulate organic carbon export at high temporal resolution in the eastern Fram Strait: influence of Atlantic Water on flux composition. *Mar Ecol Prog Ser* **440**: 127–136. DOI: <https://doi.org/10.3354/meps09385>
- Lalande, C, Nöthig, E-M, Somavilla, R, Bauerfeind, E, Shevshenko, V and Okolodkov, Y.** 2014. Variability in under-ice export fluxes of biogenic matter in the Arctic Ocean. *Glob Biogeochem Cycle* **28**: 571–583. DOI: <https://doi.org/10.1002/2013GB004735>
- Lancelot, C.** 1995. The mucilage phenomenon in the continental coastal waters of the North Sea. *Sci Total Environ.* **165**(1): 83–102. DOI: [https://doi.org/10.1016/0048-9697\(95\)04545-C](https://doi.org/10.1016/0048-9697(95)04545-C)
- Laney, SR and Sosik, HM.** 2014. Phytoplankton assemblage structure in and around a massive under-ice bloom in the Chukchi Sea. *Deep Sea Res Pt 2* **105**: 30–41. DOI: <https://doi.org/10.1016/j.dsr2.2014.03.012>
- Latasa, M.** 2007. Improving estimations of phytoplankton class abundances using CHEMTAX. *Mar Ecol Prog Ser* **329**: 13–21. DOI: <https://doi.org/10.3354/meps329013>
- Legendre, L, Gosselin, M, Hirche, HJ, Kattner, G and Rosenberg, G.** 1993. Environmental control and potential fate of size-fractionated phytoplankton production in the Greenland Sea (75°N). *Mar Ecol Prog Ser* **98**(3): 297–313. DOI: <https://doi.org/10.3354/meps098297>
- Mackey, MD, Mackey, DJ, Higgins, HW and Wright, SW.** 1996. CHEMTAX – a program for estimating class abundances from chemical markers: application to HPLC measurements of phytoplankton. *Mar Ecol Prog Ser* **144**: 265–283. DOI: <https://doi.org/10.3354/meps144265>
- Massicotte, P, Amiraux, R, Amyot, MP, Archambault, P, Ardyna, M, Arnaud, L, Artigue, L, Aubry, C, Ayotte, P, Bécu, G, Bélanger, S, Benner, R, Bittig, HC, Bricaud, A, Brossier, É, Bruyant, F, Chauvaud, L, Christiansen-Stowe, D, Claustre, H, Cornet-Barthaux, V, Coupel, P, Cox, C, Delaforge, A, Dezutter, T, Dimier, C, Domine, F, Dufour, F, Dufresne, C, Dumont, D, Ehn, J, Else, B, Ferland, J, Forget, MH, Fortier, L, Galí, M, Galindo, V, Gallinari, M, Garcia, N, Gérikas Ribeiro, C, Gourdal, M, Gourvil, P, Goyens, C, Grondin, PL, Guillot, P, Guilmette, C, Houssais, MN, Joux, F, Lacour, L, Lacour, T, Lafond, A, Lagunas, J, Lalande, C, Laliberté, J, Lambert-Girard, S, Larivière, J, Lavaud, J, LeBaron, A, Leblanc, K, Le Gall, F, Legras, J, Lemire, M, Levasseur, M, Leymarie, E, Leynaert, A, Lopes dos Santos, A, Lourenço, A, Mah, D, Marec, C, Marie, D, Martin, N, Marty, C, Marty, S, Massé, G, Matsuoka, A, Matthes, L, Moriceau, B, Muller, PE, Mundy, CJ, Neukermans, G, Oziel, L, Panagiotopoulos, C, Pangrazi, JJ, Picard, G, Picheral, M, Pinczon du Sel, F, Pogorzelec, N, Probert, I, Quéguiner, B, Raimbault, P, Ras, J, Rehm, E, Reimer, E,**

- Rontani, JF, Rysgaard, S, Saint-Béat, B, Sampei, M, Sansoulet, J, Schmechtig, C, Schmidt, S, Sempéré, R, Sévigny, C, Shen, Y, Tragin, M, Tremblay, JÉ, Vulot, D, Verin, G, Vivier, F, Vladioiu, A, Whitehead, J and Babin, M.** 2020. Green Edge ice camp campaigns: understanding the processes controlling the under-ice Arctic phytoplankton spring bloom. *Earth Syst Sci Data* **12**(1): 151–176. DOI: <https://doi.org/10.5194/essd-12-151-2020>
- Matrai, PA, Olson, E, Suttles, S, Hill, V, Codispoti, LA, Light, B and Steele, M.** 2013. Synthesis of primary production in the Arctic Ocean: I. Surface waters, 1954–2007. *Prog Oceanogr* **110**: 93–106. DOI: <https://doi.org/10.1016/j.pocean.2012.11.004>
- Mayot, N, Matrai, P, Ellingsen, IH, Steele, M, Johnson, K, Riser, SC and Swift, D.** 2018. Assessing phytoplankton activities in the seasonal ice zone of the Greenland Sea over an annual cycle. *J Geophys Res Oceans* **123**(11): 8004–8025. DOI: <https://doi.org/10.1029/2018JC014271>
- Michel, C, Legendre, L, Ingram, RG, Gosselin, M and Levasseur, M.** 1996. Carbon budget of sea-ice algae in spring: Evidence of a significant transfer to zooplankton grazers. *J Geophys Res Oceans* **101**(C8): 18345–18360. DOI: <https://doi.org/10.1029/96JC00045>
- Mills, MM, Brown, ZW, Laney, SR, Ortega-Retuerta, E, Lowry, KE, van Dijken, GL and Arrigo, KR.** 2018. Nitrogen limitation of the summer phytoplankton and heterotrophic prokaryote communities in the Chukchi Sea. *Front Mar Sci* **5**(362). DOI: <https://doi.org/10.3389/fmars.2018.00362>
- Moberg, EA and Sosik, HM.** 2012. Distance maps to estimate cell volume from two-dimensional plankton images. *Limnol Oceanogr Methods* **10**(4): 278–288. DOI: <https://doi.org/10.4319/lom.2012.10.278>
- Mousing, EA, Richardson, K and Ellegaard, M.** 2018. Global patterns in phytoplankton biomass and community size structure in relation to macronutrients in the open ocean. *Limnol Oceanogr* **63**(3): 1298–1312. DOI: <https://doi.org/10.1002/lno.10772>
- Mundy, CJ, Gosselin, M, Ehn, J, Gratton, Y, Rossnagel, A, Barber, DG, Martin, J, Tremblay, J-É, Palmer, M, Arrigo, KR, Darnis, G, Fortier, L, Else, B and Papakyriakou, T.** 2009. Contribution of under-ice primary production to an ice-edge upwelling phytoplankton bloom in the Canadian Beaufort Sea. *Geophys Res Lett* **36**: L17601. DOI: <https://doi.org/10.1029/2009GL038837>
- Mundy, CJ, Gosselin, M, Gratton, Y, Brown, K, Galindo, V, Campbell, K, Levasseur, M, Barber, D, Papakyriakou, T and Bélanger, S.** 2014. Role of environmental factors on phytoplankton bloom initiation under landfast sea ice in Resolute Passage, Canada. *Mar Ecol Prog Ser* **497**: 39–49. DOI: <https://doi.org/10.3354/meps10587>
- Newton, R, Schlosser, P, Mortlock, R, Swift, J and MacDonald, R.** 2013. Canadian Basin freshwater sources and changes: Results from the 2005 Arctic Ocean Section. *J Geophys Res Oceans* **118**(4): 2133–2154. DOI: <https://doi.org/10.1002/jgrc.20101>
- Nicolaus, M, Katlein, C, Maslanik, J and Hendricks, S.** 2012. Changes in Arctic sea ice result in increasing light transmittance and absorption. *Geophys Res Lett* **40**(11): 2699–2700. DOI: <https://doi.org/10.1029/2012GL053738>
- Nöthig, E-M, Bracher, A, Engel, A, Metfies, K, Niehoff, B, Peeken, I, Bauerfeind, E, Cherkasheva, A, Gäbler-Schwarz, S, Hardge, K, Kiliyas, E, Kraft, A, Kidane, YM, Lalande, C, Piontek, J, Thomisch, K and Wurst, M.** 2015. Summertime plankton ecology in Fram Strait—a compilation of long- and short-term observations. *Polar Res* **34**(1): 23349. DOI: <https://doi.org/10.3402/polar.v34.23349>
- Olson, RJ and Sosik, HM.** 2007. A submersible imaging-in-flow instrument to analyze nano- and microplankton: Imaging FlowCytobot. *Limnol Oceanogr Methods* **5**(6): 195–203. DOI: <https://doi.org/10.4319/lom.2007.5.195>
- Oziel, L, Massicotte, P, Randelhoff, A, Ferland, J, Vladioiu, A, Lacour, L, Galindo, V, Lambert-Girard, S, Dumont, D, Cuypers, Y, Bouruet-Aubertot, P, Mundy, C-J, Ehn, J, Bécu, G, Marec, C, Forget, M-H, Garcia, N, Coupel, P, Raimbault, P, Houssais, M-N and Babin, M.** 2019. Environmental factors influencing the seasonal dynamics of under-ice spring blooms in Baffin Bay. *Elem Sci Anth* **7**(34). DOI: <https://doi.org/10.1525/elementa.372>
- Pavlov, AK, Taskjelle, T, Kauko, HM, Hamre, B, Hudson, SR, Assmy, P, Duarte, P, Fernández-Méndez, M, Mundy, CJ and Granskog, MA.** 2017. Altered inherent optical properties and estimates of the underwater light field during an Arctic under-ice bloom of *Phaeocystis pouchetii*. *J Geophys Res Oceans* **122**(6): 4939–4961. DOI: <https://doi.org/10.1002/2016JC012471>
- Picheral, M, Colin, S and Irisson, JO.** 2017. EcoTaxa, a tool for the taxonomic classification of images. Available at <http://ecotaxa.obs-vlfr.fr>.
- Randelhoff, A, Holding, J, Janout, M, Sejr, MK, Babin, M, Tremblay, J-É and Alkire, MB.** 2020. Pan-Arctic Ocean primary production constrained by turbulent nitrate fluxes. *Front Mar Sci* **7**(150). DOI: <https://doi.org/10.3389/fmars.2020.00150>
- Randelhoff, A, Oziel, L, Massicotte, P, Bécu, G, Galí, M, Lacour, L, Dumont, D, Vladioiu, A, Marec, C, Bruyant, F, Houssais, M-N, Tremblay, J-É, Deslongchamps, G and Babin, M.** 2019. The evolution of light and vertical mixing across a phytoplankton ice-edge bloom. *Elem Sci Anth* **7**(1): 20. DOI: <https://doi.org/10.1525/elementa.357>
- Ray, JL, Skaar, KS, Simonelli, P, Larsen, A and others.** 2016. Molecular gut content analysis demonstrates that *Calanus* grazing on *Phaeocystis pouchetii* and *Skeletonema marinoi* is sensitive to bloom phase but not prey density. *Mar Ecol Prog Ser* **542**: 63–77. DOI: <https://doi.org/10.3354/meps11560>
- Reigstad, M and Wassmann, P.** 2007. Does *Phaeocystis* spp. contribute significantly to vertical export of

- organic carbon? *Biogeochemistry* **83**(1): 217–234. DOI: <https://doi.org/10.1007/s10533-007-9093-3>
- Renaut, S, Devred, E and Babin, M.** 2018. Northward expansion and intensification of phytoplankton growth during the early ice-free season in Arctic. *Geophys Res Lett* **45**(19): 10,590–10,598. DOI: <https://doi.org/10.1029/2018GL078995>
- Rey, F.** 2012. Declining silicate concentrations in the Norwegian and Barents Seas. *ICES J Mar Sci* **69**(2): 208–212. DOI: <https://doi.org/10.1093/icesjms/fss007>
- Saiz, E, Calbet, A, Isari, S, Antó, M, Velasco, EM, Almeda, R, Movilla, J and Alcaraz, M.** 2013. Zooplankton distribution and feeding in the Arctic Ocean during a *Phaeocystis pouchetii* bloom. *Deep Sea Res Pt 1* **72**: 17–33. DOI: <https://doi.org/10.1016/j.dsr.2012.10.003>
- Sakshaug, E.** 2004. Primary and secondary production in the Arctic Sea. In: Stein, R and MacDonald, RW (eds.), *The Organic Carbon Cycle in the Arctic Ocean*, 57–81. Berlin: Springer. DOI: https://doi.org/10.1007/978-3-642-18912-8_3
- Schoemann, V, Becquevort, S, Stefels, J, Rousseau, V and Lancelot, C.** 2005. *Phaeocystis* blooms in the global ocean and their controlling mechanisms: a review. *J Sea Res* **53**(1): 43–66. DOI: <https://doi.org/10.1016/j.seares.2004.01.008>
- Simo-Matchim, AG, Gosselin, M, Poulin, M, Ardyna, M and Lessard, S.** 2017. Summer and fall distribution of phytoplankton in relation to environmental variables in Labrador fjords, with special emphasis on. *Phaeocystis pouchetii*. *Mar Ecol Prog Ser* **572**: 19–42. DOI: <https://doi.org/10.3354/meps12125>
- Simon, N, Foulon, E, Grulois, D, Six, C, Desdevises, Y, Latimier, M, Le Gall, F, Tragin, M, Houdan, A, Derelle, E, Jouenne, F, Marie, D, Le Panse, S, Vulot, D and Marin, B.** 2017. Revision of the genus *Micromonas* Manton et Parke (Chlorophyta, Mamielophyceae), of the type species *M. pusilla* (Butcher) Manton & Parke and of the species *M. commoda* van Baren, Bachy and Worden and description of two new species based on the genetic and phenotypic characterization of cultured isolates. *Protist* **168**(5): 612–635. DOI: <https://doi.org/10.1016/j.protis.2017.09.002>
- Smith, WO, Codispoti, LA, Nelson, DM, Manley, T, Buskey, EJ, Niebauer, HJ and Cota, GF.** 1991. Importance of *Phaeocystis* blooms in the high-latitude ocean carbon cycle. *Nature* **352**(6335): 514–516. DOI: <https://doi.org/10.1038/352514a0>
- Sosik, HM and Olson, RJ.** 2007. Automated taxonomic classification of phytoplankton sampled with imaging-in-flow cytometry. *Limnol Oceanogr Methods* **5**(6): 204–216. DOI: <https://doi.org/10.4319/lom.2007.5.204>
- Strass, VH and Nöthig, E-M.** 1996. Seasonal shifts in ice edge phyto plankton blooms in the Barents Sea related to the water column stability. *Polar Biol* **16**(6): 409–422. DOI: <https://doi.org/10.1007/BF02390423>
- Stroeve, J and Notz, D.** 2018. Changing state of Arctic sea ice across all seasons. *Environ Res Lett* **13**(10): 103001. DOI: <https://doi.org/10.1088/1748-9326/aade56>
- Takeda, S.** 1998. Influence of iron availability on nutrient consumption ratio of diatoms in oceanic waters. *Nature* **393**: 25. DOI: <https://doi.org/10.1038/31674>
- Tremblay, G, Belzile, C, Gosselin, M, Poulin, M, Roy, S and Tremblay, J-É.** 2009. Late summer phytoplankton distribution along a 3500 km transect in Canadian Arctic waters: strong numerical dominance by picoeukaryotes. *Aquat Microb Ecol* **54**(1): 55–70. DOI: <https://doi.org/10.3354/ame01257>
- Tremblay, J-É and Gagnon, J.** 2009. The effects of irradiance and nutrient supply on the productivity of Arctic waters: a perspective on climate change. In: Nihoul, JCJ and Kostianoy, AG (eds.), *Influence of Climate Change on the Changing Arctic and Sub-Arctic Conditions*, 73–93. Dordrecht, Netherlands: Springer. DOI: https://doi.org/10.1007/978-1-4020-9460-6_7
- Tremblay, J-É, Hattori, H, Michel, C, Ringuette, M, Mei, Z-P, Lovejoy, C, Fortier, L, Hobson, KA, Amiel, D and Cochran, K.** 2006. Trophic structure and pathways of biogenic carbon flow in the eastern North Water Polynya. *Prog Oceanogr* **71**(2–4): 402–425. DOI: <https://doi.org/10.1016/j.pocean.2006.10.006>
- Tremblay, J-É, Simpson, K, Martin, J, Miller, L, Gratton, Y, Barber, D and Price, NM.** 2008. Vertical stability and the annual dynamics of nutrients and chlorophyll fluorescence in the coastal, southeast Beaufort Sea. *J Geophys Res* **113**(C7): C07S90. DOI: <https://doi.org/10.1029/2007JC004547>
- Tschudi, M, Meier, WN, Stewart, JS, Fowler, C and Maslanik, J.** 2019. *EASE-Grid Sea Ice Age, Version 4*. [1984–2018]. Boulder, Colorado USA: NASA National Snow and Ice Data Center Distributed Active Archive Center. DOI: <https://doi.org/10.5067/UTAV7490FEPB>
- Vidussi, F, Roy, S, Lovejoy, C, Gammelgaard, M, Thomsen, HA, Booth, B, Tremblay, J-É and Mostajir, B.** 2004. Spatial and temporal variability of the phytoplankton community structure in the North Water Polynya, investigated using pigment biomarkers. *Can J Fish Aquat Sci* **61**(11): 2038–2052. DOI: <https://doi.org/10.1139/f04-152>
- Wassmann, P.** 1994. Significance of sedimentation for the termination of *Phaeocystis* blooms. *J Mar Syst* **5**(1): 81–100. DOI: [https://doi.org/10.1016/0924-7963\(94\)90018-3](https://doi.org/10.1016/0924-7963(94)90018-3)
- Wassmann, P, Peinert, R and Smetacek, V.** 1991. Patterns of production and sedimentation in the boreal and polar Northeast Atlantic. *Polar Res* **10**(1): 209–228. DOI: <https://doi.org/10.1111/j.1751-8369.1991.tb00647.x>
- Wilson, SE, Swalethorp, R, Kjellerup, S, Wolverton, MA, Ducklow, HW and Yager, PL.** 2015. Meso- and macro-zooplankton community structure of the

- Amundsen Sea Polynya, Antarctica (Summer 2010–2011). *Elem Sci Anth* **3**: 000033. DOI: <https://doi.org/10.12952/journal.elementa.000033>
- Wollenburg, JE, Katlein, C, Nehrke, G, Nöthig, EM, Matthiessen, J, Wolf-Gladrow, DA, Nikolopoulos, A, Gázquez-Sánchez, F, Rossmann, L, Assmy, P, Babin, M, Bruyant, F, Beaulieu, M, Dybwad, C and Peeken, I.** 2018. Ballasting by cryogenic gypsum enhances carbon export in a *Phaeocystis* under-ice bloom. *Sci Rep* **8**(1): 7703. DOI: <https://doi.org/10.1038/s41598-018-26016-0>
- Wright, SW, Ishikawa, A, Marchant, HJ, Davidson, AT, van den Enden, RL and Nash, GV.** 2009. Composition and significance of picophytoplankton in Antarctic waters. *Polar Biol* **32**(5): 797–808. DOI: <https://doi.org/10.1007/s00300-009-0582-9>
- Yager, PL, Connelly, TL, Mortazavi, B, Wommack, KE, Bano, N, Bauer, JE, Opsahl, S and Hollibaugh, JT.** 2001. Dynamic bacterial and viral response to an algal bloom at subzero temperatures. *Limnol Oceanogr* **46**(4): 790–801. DOI: <https://doi.org/10.4319/lo.2001.46.4.0790>

How to cite this article: Ardyna, M, Mundy, CJ, Mills, MM, Oziel, L, Grondin, P-L, Lacour, L, Verin, G, van Dijken, G, Ras, J, Alou-Font, E, Babin, M, Gosselin, M, Tremblay, J-É, Raimbault, P, Assmy, P, Nicolaus, M, Claustre, H and Arrigo, KR. 2020. Environmental drivers of under-ice phytoplankton bloom dynamics in the Arctic Ocean. *Elem Sci Anth*, **8**: 30. DOI: <https://doi.org/10.1525/elementa.430>

Domain Editor-in-Chief: Jody W. Deming, School of Oceanography, University of Washington, US

Knowledge Domain: Ocean Science

Part of an *Elementa* Special Feature: Green Edge

Submitted: 14 February 2020 **Accepted:** 02 June 2020 **Published:** 09 July 2020

Copyright: © 2020 The Author(s). This is an open-access article distributed under the terms of the Creative Commons Attribution 4.0 International License (CC-BY 4.0), which permits unrestricted use, distribution, and reproduction in any medium, provided the original author and source are credited. See <http://creativecommons.org/licenses/by/4.0/>.



Elem Sci Anth is a peer-reviewed open access journal published by University of California Press.

OPEN ACCESS